NTNU – Trondheim
Norwegian University of
Science and Technology

Estimating the roughness factor using Lidar scanning system

Comparison of tunnel surfaces before and after applied shotcrete

Ann-Kristin Selmer

Geotechnology
Submission date: Januar 2014
Supervisor: Charlie Chunlin Li, IGB
Co-supervisor: Elin Kathrine Morgan, NGI

Norwegian University of Science and Technology
Department of Geology and Mineral Resources Engineering

Acknowledgement

This thesis is written in connection to a project at the Norwegian Geotechnical Institute, and there are several people I would like to thank. First of all, thanks to my supervisor Elin Katrine Morgan for all the support and help during this work. Thank you for giving me constructive feedback of ways to take on this task and keeping me motivated. Also thanks to Heidi Hefre Haugland and Helge Christian Smebye for helping me when I was stuck with problems. In addition to all the people at the Norwegian Geotechnical Institute in Trondheim: thank you for having an office available for me and for every lunch break together. It has been a pleasure getting to know you.

Thank you to Charlie C. Li for being a true inspiration during my studying years at NTNU. You give me motivation and are always helpful and smiling.

To my two kids; thank you for just being here and giving me joy and laughter. Last but not least, thanks to my husband; thank you for sticking up with me all these months. You have been a major support.

Ann Kristin Selmer

Trondheim, January 2014

Abstract

This thesis gives a suggestion of a method for extracting the roughness factor for estimating the sprayed concrete volume in tunnel applications. The determination of the roughness factor today is based on experience and is usually done by guessing or based on the roughness factor used in the previous blasted round. This study includes creating a look-up-chart which could enable the contractor and engineer to have a better foundation and documentation on why the roughness factor is chosen as it is. This is performed by using LiDAR scanning system and using the LiDAR data from the rock mass surface from a water cavern close to Lillestrøm in Norway.

A comparison of the LiDAR data and the hand mapped data is performed, regarding special features in the rock mass, such as geometry, major structures and weakness zones. The LiDAR data display the true surface of the rock mass and visualizing geometry is possible with the LiDAR model. Measurements of the generated profiles in the cavern have been performed on selected areas extracting roughness factor between the rock mass surface and the sprayed concrete surface. Calculating the roughness factor using profile length is a cumbersome method to use due to the holes in the data. It is recommended that the Lidar model is as watertight as possible and this requires more precise processing of the data.

The calculated average roughness factors have been correlated to the corresponding Q-value, the RQD/J_n-quotient, RQD and the joint set number J_n. From the results of the correlation it is suggested to use the Q-value and the joint set number J_n as a basis for the look-up-chart. Generally the results indicate that the roughness factor increases with decreasing Q-value. In addition it could be seen that the roughness factor value increased with approximately 0,2 for every increasing value of the joint set number. It must be emphasized that this is a suggestion based on only one test site. The method used to find the roughness factor is recommended evaluated. It may be possible that large scale roughness requires a larger roughness factor to meet the requirement of minimum sprayed concrete thickness. Further studies are necessary.

Sammendrag

Denne oppgaven gir et forslag på en fremgangsmåte for å finne ruhetsfaktoren for estimering av volum av sprøytebetong i tunnelsammenheng. Bestemmelsen av ruhetsfaktoren i dag er gjort ved gjetning og ofte blir ruhetsfaktoren fra forrige salve brukt. Denne studien inkluderer å lage et «look-up»-diagram som kan gjøre det mulig for entreprenøren og ingeniøren å ha bedre grunnlag for bestemmelse av ruhetsfaktoren og kunne dokumentere hvorfor ruhetsfaktoren er valgt som den er. Dette er gjort ved hjelp av LiDAR data fra bergoverflaten fra en fjellhall nær Lillestrøm i Norge.

En sammenligning av LiDAR data og håndkartlagt data er utført, med hensyn på spesielle kjennetegn i bergmassen som for eksempel geometri, større strukturer og svakhetssoner. LiDAR data viser den sanne overflaten av bergmassen og dermed er visualisering av geometrien på overflaten mulig. Målinger av de genererte profilene har blitt utført på utvalgte områder i fjellhallen og med det en beregning av ruhetsfaktor mellom bergmasseoverflaten og overflaten til sprøytebetongen. Beregningen av ruhetsfaktoren ved hjelp av profillengde er mulig, men en tungvint metode å bruke på grunn av alle hullene i modellen. Det anbefales at LiDAR-modeller er så vanntett som mulig, men dette krever mer presis prosessering av dataene.

Gjennomsnittlige ruhetsfaktorer er korrelert med tilsvarende Q - verdi, RQD / J_n - kvotienten, RQD og sprekkesettnummeret J_n. Fra resultatene av korrelasjonen er det foreslått å bruke Q-verdien og sprekkesettnummeret J_n som grunnlag for «look-up»-diagrammet. Generelt viser resultatene at ruhetsfaktoren øker med avtagende Q - verdi. I tillegg kan det ses at verdien på ruhetsfaktoren økte med omtrent 0,2 for hver økende verdi av sprekkesettnummeret. Det må understrekes at dette er et forslag basert på kun én lokalitet. Metoden som brukes for å finne ruhetsfaktoren anbefales å vurdere videre. Det kan være mulig at storskala ruhet krever en større ruhetsfaktor for å oppfylle kravet om minimum sprøytebetongtykkelse. Ytterligere studier er nødvendig.

Contents

1 Introduction

1.1 Motivation

In recent years there have been several serious accidents related to rock mass engineering in Norway. Examples include the collapse in Hanekleiv tunnel in Buskerud, on the 25 December 2006 (Carstens 2007), and later a rock fall in Oslofjordtunnelen (Nilsen 2010), which led to a collapse of the tunnel roof during construction. These among other incidents have led to stricter requirements concerning tunnel operations before, during and after excavation when it comes to documentation of rock support.

Today, the Norwegian Method of Tunneling (NMT) is used as a conventional method for drill and blast technique in hard rock. The main principle is that the rock support is designed for the actual ground conditions, and requires a continuous assessment of the rock mass quality (Palmstrøm and Naas 1993). After each blasted round, an engineering geologist is on site to make an assessment of the rock mass quality. Based on this assessment the rock mass support is determined, including number of bolts, bolting patterns and the recommended thickness of sprayed concrete.

To meet the requirements of minimum sprayed concrete thickness, the roughness factor needs to be taken into account. Today, there is no precise method for determining the roughness factor. One way is back calculation of the roughness factor based on drilled cores for determining thickness of sprayed concrete. Another is using the roughness factor from the previous blasted round and also by guessing the roughness factor. Guessing the roughness factor can often be inaccurate, both for safety and economic reasons. It is therefore a request to find a method for estimating the roughness factor, and be able to make a better foundation and documentation of why the roughness factor is chosen as it is.

1.2 Background

The LiDAR scanning system is a laser scanning technique that maps surfaces of blasted excavations and rock outcrops. LiDAR stands for light detection and range, and uses a laser beam to measure the distance from an object to the scanner (Harrap and Lato 2010). In a relative short amount of time, it can give a representative 3D image of the surface. The uses of this equipment are many; excavation volume and dimension control, deformation control, surface inspections, structural analysis and maintenance, free-form components inspection, built environment and construction progress monitoring (LiDAR UK 2014).

In tunnel applications LiDAR has been proven as helpful tool for deformation measurements (GIM International 2009), block geometry characterization (Fekete et al. 2010), characterization and documentation of rock faces and outcrops (Haugland 2010), discontinuity measurements (Haugland 2010), and also a tool for measuring applied sprayed concrete thickness (Fekete et al. 2010).

In tunnel applications it is of great importance that the mean applied sprayed concrete thickness is satisfied. This requires a precise calculation of the sprayed concrete volume and at the same time take into account the roughness of the tunnel surface. LiDAR data provides a true image of the rock mass surface and hence also display a true roughness of the rock mass. It is based on this anticipated that the LiDAR technology can be a helpful tool for determining the roughness factor.

1.3 Purpose and scope of study

This study is a master thesis in the subject TGB4930, engineering geology and rock mechanics at the Norwegian University of Science (NTNU) and is done in collaboration with Norwegian Geotechnical Institute (NGI). The main task is to see if it is possible to find a method for estimating a more precise roughness factor for determining the right amount of sprayed concrete ordered for each blasted round. This will be done by calculating the roughness factor from the scanned surfaces before and after applied sprayed concrete, from a water storage cavern in Lillestrøm, Norway. The calculated roughness factor for this cavern will be correlated to

determined features in the rock mass and used as a basis for further suggestions for values and boundaries for a look-up-chart. The look-up-chart can enable the contractor and engineer to better estimate the roughness factor when calculating the required sprayed concrete volume corresponding to a given Q-value.

To assess the suitability of using LiDAR for roughness factor analysis, an evaluation of the application for geological mapping is performed by comparing the manually mapped tunnel sections with corresponding sections in the LiDAR data with special regard to geometry, major structures and weakness zones.

The cavern is scanned with a LiDAR scanning system, including the rock surface before applied sprayed concrete and the surface after applied sprayed concrete. The extraction of the roughness factor is by dividing the measured profile lengths before and after applied sprayed concrete. This analysis will include an evaluation on the method used for calculating the roughness factor.

The limitations and errors associated with the calculation will be assessed, together with a discussion whether this method for determination of the roughness factor is realistic.

1.4 Thesis structure

In order to use LiDAR data for calculating the roughness factor for rock mass surfaces, it is necessary to have knowledge about the rock mass behavior and the terrestrial Lidar scanning system. This is provided in Chapters 2 and 3, respectively. In Chapter 4, an overview of the scanning site is given together with a description of the geological features of the cavern. Chapter 5 presents the comparison of the hand mapped data and the LiDAR data of the cavern, the method used for calculating the roughness factor and also suggestions for creating a look-up-chart for a better estimation of the roughness factor. The results of the analysis performed are provided in Chapter 6. Chapter 7 presents the discussions and limitations of the study. Finally, the conclusions and suggested further work are given in Chapter 8.

2 Rock mass characteristics, the Q system and determination of rock support

This chapter will examine the theory behind classification of the rock masses and the method used for determining the recommended rock support. It will address the main properties to look for when describing rock masses and how it is documented. It will address the description of the rock mass classification systems, in the level needed for this thesis, and how to determine the amount of rock support and sprayed concrete based on a given rock mass class. It will also address the roughness of tunnel surfaces and the application of sprayed concrete.

The method for excavating tunnels used today is The Norwegian Method of Tunneling (NMT), where drill and blasting are the most common method of excavation. It is a cost efficient and effective method for excavating in hard rock where jointing and overbreak are dominant (NGI 2013b). It emphasizes the importance of thorough descriptions and documentations of the projects geological and geotechnical aspects. The main principle for the NMT is that the rock support is designed for the actual ground conditions, which requires a continuous assessment of the rock mass quality and flexible support methods (Palmstrøm and Naas 1993). It uses the combination of systematic bolting and sprayed concrete application based on description of the rock mass surface using among others the Q-system.

2.1 Geological mapping and classification of the rock mass using the Q–system

In all the stages of underground excavation today, the documentation of rock mass quality must be thorough. Both during planning and during excavation as the tunnel face is progressing, geological mapping is conducted to give a description of the rock masses. NMT emphasizes the geological assessment of the rock mass and uses classification systems to describe the rock surface. With respect to stability of the tunnel, the description of the rock mass is of key importance. The mapping consists of describing features from the rock surface to a piece of paper. During about 30 minutes the engineering geologist on site will determinate the rock type, evaluate the rock quality, and extract strike and dip direction of typical fractures, wedges and

weakness zones. The manually drafted map represents the surface of the tunnel where the tunnel is seen from above with the wall folded out, the sides of the drawing are the wall and the middle section is the crown of the tunnel.

A classification system is a very useful and practical engineering tool, not only because it provides a starting point for the design of tunnel support but also because it forces the users to examine the properties of the rock mass in a very systematic manner. Most of these classification systems are based on empirical relations between rock mass parameters and engineering applications, such as tunnels, slopes, foundations, and excavatability. The purpose of these systems is to provide understanding of how the rock mass behaves, gives guidelines for engineering support design and also provides a common basis for communication between engineer and geologist.

In 1974, the Norwegian Geotechnical Institute (NGI) developed the Q-system based on over 200 tunnel case histories, mainly from Scandinavia (Barton et al 1974). The system was upgraded in 1993 after incorporating over a 1000 case studies (Grimstad and Barton 1993). The Q-system is a quantitative classification system for estimating rock-support, based on numerical approximations of rock quality. The value of Q depends on the underground opening and its geometry, and it therefore not an independent characterization of the rock (NGI 2013).

There are six rock mass parameters that have to be estimated. From these parameters rock quality Q is defined as:

$$Q = \frac{RQD}{J_n} \times \frac{J_r}{J_a} \times \frac{J_w}{SRF}$$

The Q-values ranges from 0.0001 for exceptionally poor quality to 1000 for exceptionally good quality rock, and is used to define the categories of rock. The first paragraph of the equation is the overall structure of the rock mass, and the quotient is a relative measure of the block size. The second is a measure of roughness and frictional characterization of the joint walls or filling material between the blocks. The third paragraph is an empirical factor described as the rock stress influence. The different Q-values relate to different types of permanent rock support found in a schematic support chart, presented in Figure 2-1. The Q-value is related to rock support by defin-

ing the corresponding dimension for underground excavation. This dimension is again a function of size and the type of excavation.

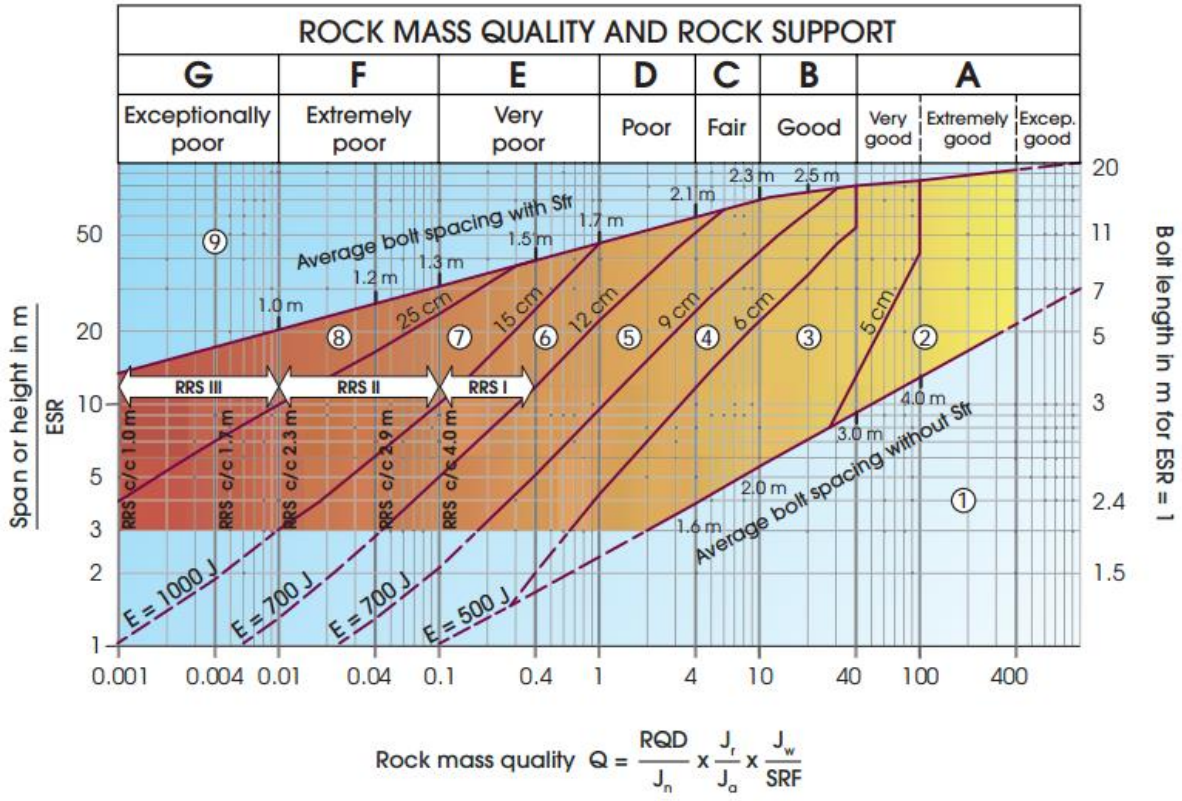

Figure 2-1: The Q-system rock support chart (Norwegian Geotechnical Institute 2013a)

The RQD factor is a measure for the degree of jointing or block size in the rock mass. It is by definition the length in percent of measured length of unweathered drilled core bits longer than 10 cm (Palmstrøm and Broch 2006). When drill cores are not available, the RQD can be performed by measuring in the same way on a 1 m section on the rock mass surface. The joint set number J_n is defined by the number of joint sets present in the rock mass.

Geological mapping is conducted after each blasted round; after mechanical- and manual scaling and before the application of sprayed concrete. It is important that there is allocated sufficient time for geological mapping and normally the geologist on site has about 30 minutes to perform this (Norwegian Public Roads Administration, 2013). The classification and mapping should in-

clude determination of rock type, structures, geometry of fractures and also the orientation, width and possible clay content of weakness zones. Based on the classification of the rock mass a support class is defined. The support should be documented on paper or electronically by describing the type of support, the amount and placement.

2.2 Rock mass stability

Understanding the failure mechanism of a rock mass surrounding an under-ground opening is essential in the design of support systems. The failure mechanism depends on the in situ stress level and characteristics of the given rock mass. At shallow depths, where the rock mass may be blocky and jointed, the stability problems are generally associated with gravity falls of blocks and wedges from the roof and side walls, since the rock confinement is generally low. As the depth below the ground surface increases, the rock stress increases and may reach a level at which the failure of the rock mass is induced. At the same insufficient horizontal stresses may also lead to rock mass failure. To prevent rock mass failure, the features of the rock masses have to be known. It is characteristic for the rock mass to be jointed and usually about 3 to 5 % of the total length of a tunnel or cavern is influences by weakness zones (Norwegian Public Roads Administration 2013). Besides being inhomogeneous and anisotropic they are also discontinuous.

The stability rating of rock masses both in underground excavations and slope stability, often the fact that materials are discontinuous or jointed, overshadow other material properties such as rock strength. By performing geological mapping, the details of the rock material are described, and consist of mapping details and the natural fractures. The Q-system itself cannot evaluate the stability of single rock or larger wedges. These are controlled by the geometry and the orientation of the fractures. Therefore it is of importance to perform a general geological mapping with details of the fractures, such as orientation, persistence, spacing, thickness, filling, waviness and unevenness for each set. The fractures of most interest are those with approximately the same strike as the tunnel axis, but with variable dip directions (Løset 1997). These can cause block or wedge failure and are described in the pictures a) to d) in Figure 2-2.

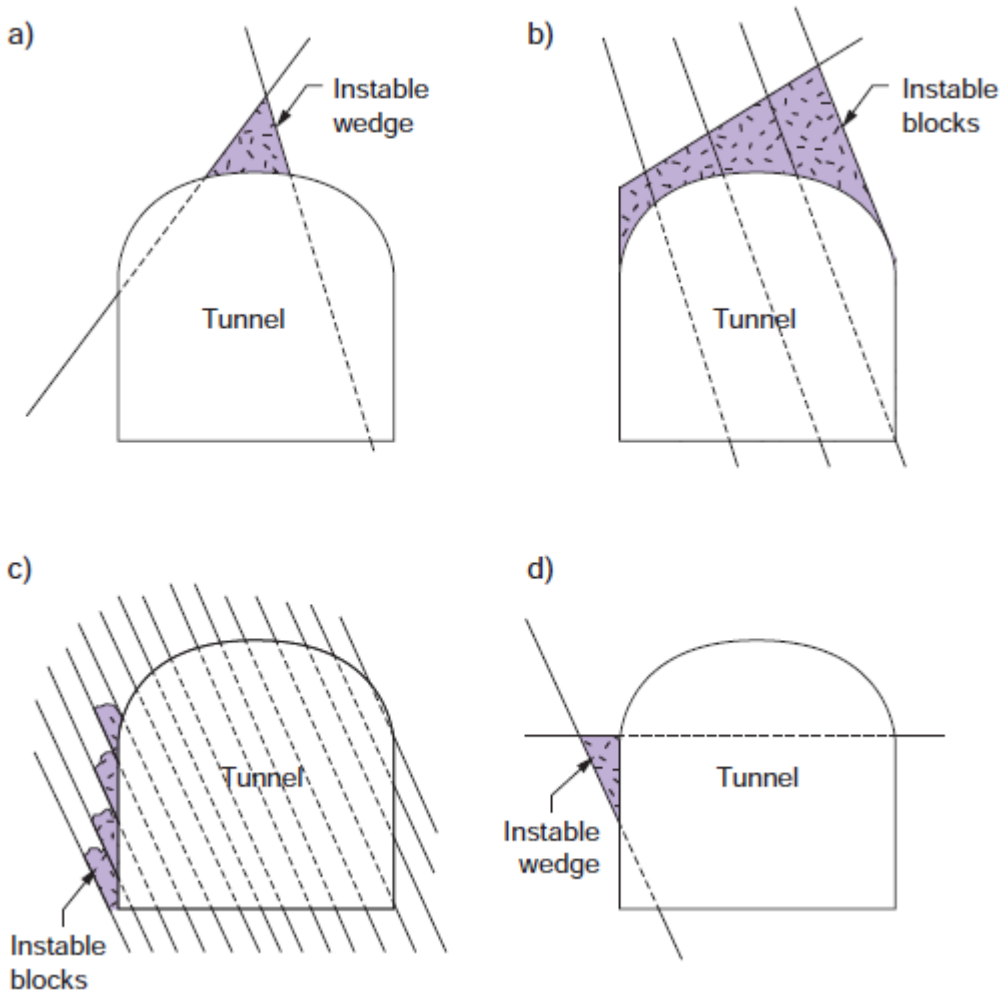

Figure 2-2: Different stability problems due to unfavorable discontinuity orientation (Løset 1997)

The rock mass is then described by block shape, block size, and discontinuity conditions. It can be divided into small or large blocks, caused by some fractures, and can fall or slide down from the excavation boundaries. Data collected from the mapping of these structures are used to determine the orientation of the major joint sets and to assess the potential modes of structural failure (Hoek et al 1993).

The fracturing of rock is primarily formed by the natural stresses the rock masses have been exposed to, and usually form a specific pattern, for example joints, fractures, stings and detailed fractures. Small fractures and stings can also be made from the strains the rock masses is exposed to during mining and construction operations, for example by blasting or by stress concentration

in nearby rock masses. The orientation of the fractures is some of the critical aspects in underground excavations, and requires consideration in terms of block or wedge movement or failure (Løset 1997). To stabilize blocks or wedges, and hence the opening, an important step is to determine the number, orientation and conditions of the fractures. The orientation and direction of the fractures are measured with a compass and the task for the geologist on site is to locate the most representative fractures for the rock masses in the tunnel.

In addition, the weakness zone themselves need to be evaluated. Shear zones or weakness zones are especially of great importance for the stability, both during and after excavation. They form characteristic patterns in the earth's crust and can consist of several independent sets or systems. The main directions of the weakness zones often have the same orientation as the structural jointing within the same structural area. The shear zones occur when there is a movement along the fractures, due to stresses from ether tectonic events or stresses induced by fillings in the zones. Alteration, weathering and hydrothermal activity are features that may have had a significant impact on the composition and the properties of a zone. The filling in these zones may span from crushed, brecciated and permeable material with relatively small amount of clay up to highly weathered altered, highly plastic, swelling clay gouge. They can vary in thickness from a few centimeters to several meters (Brock and Nilsen 2001).

When mapping zones of weakness or fractures, it is important to describe these zones individually from the surrounding rock mass. This is often due to the fact that the fractures are of most importance for the stability, not the rock strength itself. When a zone has been encountered, the composition and structure may be studied along with the thickness and the joint orientation. Today, a way of describe these properties is to draw them on a piece of paper and to perform a classification of the rock mass with for example the Q-system. When all these parameters are found, the decisions concerning procedure for excavation and proper rock support are prepared.

2.3 Rock support installation in tunnels

The permanent rock support in tunnels is a combination of temporary rock support determined by the entrepreneur and the rock support determined by the classification of the rock mass. The temporary supports should provide safe working environments at the face of the tunnel and

permanent support, which should meet the recommended requirement. The temporary support shall be performed so it can be included in the permanent support (Norwegian Public Roads Administration, 2013).

The most common method of rock support in Norwegian tunnels is the use of rock bolts, reinforced sprayed concrete and sprayed concrete arches. The spacing of the bolts and the sprayed concrete thickness is determined by the span or height and type of excavation and by the Q-value of the rock mass (Grimstad and Barton, 1993). The Q-support-chart basically intends to be a recommendation for rock support and no set solution. The thickness of the applied sprayed concrete is determined by the owner and has to be fulfilled by the contractor. The Norwegian Public Roads Association has recommended that there should be at least 8 mm sprayed concrete applied as minimum for rock support in addition to bolts for Norwegian mines and tunnels (Norwegian Public Roads Administration, 2010).

2.3.1 Calculation of sprayed concrete thickness

Recent years have seen an increasing use of sprayed concrete in underground excavations, particularly in poor ground conditions (Hadjigeorgiou and Charette, 2001). The sprayed concrete used today is fiber reinforced and contains alkali free accelerators to improve the application. The performance of the sprayed concrete is given in guidelines set by Norwegian Concrete Association in publication No.7 (2003).

The main task for the sprayed concrete is to hold small ”key blocks” in place so they don’t fall out, secondly to make the rock a self-bearing structure. It is often used in combination with other rock support, and should be installed so that it maintains the total support function and quality. Sprayed concrete requires a good quality-control program that should address aggregate quality, admixture, and strength, as well as application procedures and resulting rebound.

The amount of sprayed concrete is usually ordered by the contractor after every blasted round. It is calculated by the theoretical area of the rock wall and the specified thickness. In addition the volume needs to take in consideration the rebound factor and roughness factor. The rebound can be controlled by quality in workmanship of the application of sprayed concrete. Using the wrong angle, distance or composition may lead to severe rebound. By spraying of the roof the rebound

may reach 50%, but using the correct technique it is possible to keep the rebound to under 10% (Myrvang 2001).

The rough nature of the surface leads to a larger true area of the excavation than the theoretical area. This irregularity is mainly a function of natural conditions such as blockyness of the tunnel profile, orientation of the structures and filiations and also fault zones, but it can also be controlled by drill and blast processes. During application the cavities and the hollows will be filled up first before a uniformly distributed covering layer is applied. This can be taken in to account by multiplying the volume with the roughness factor. The roughness factor has to take two conditions under consideration: uneven application of sprayed concrete and the distribution of sprayed concrete on the surface. The roughness factor is determined throughout the excavation and is usually an empirical value based on experience. Other times the contractor pre-order the amount of sprayed concrete based on the previous blasted round. Due to the lack of a standardized method for determining the roughness factor, the Norwegian Concrete Association therefore refers to guessing the roughness factor. The contractor has to take measurements after the application and later adjust the factor according to the results of the control in order to meet the requirements.

The applied thickness of sprayed concrete is of importance to the stability of the excavation. Thickness control can be performed by drilling in the cured sprayed concrete in a pattern, ex of 2 x 2 m grid, measuring the thickness with a ruler. This type of control may be expensive and can take up valuable time for the project. The measurement may also be inaccurate because it they depending on where in the tunnel profile you measure the thickness.

A relatively new method for measuring the sprayed concrete thickness involves the use of Li-DAR scanning systems, by comparing a high density 2D or 3D model of the excavated tunnel to the designed tunnel (Haugland 2010). A comparison of the tunnel surface before and after applying sprayed concrete is done, by showing an error map of a specific blast round. The time it takes to extract these error maps is about 2 to 4 hours and this is mainly because of data processing.

3 LiDAR scanning system for geological applications

This part will consist of theory and the mathematical concept behind the LiDAR scanning system, and the options for making a representative model of the scanned surface. It will also address some of the issues with the scanning as well as processing the collected data. Since the method is relatively new, few studies of tunnel applications exist. However, some studies have been conducted on outcrops, and it is reasonable to assume that for tunnels, the challenges are the same.

In the current practice, much of the data collected from a site is done by manual-mapping, in the form of describing and drawing the rock masses and features. This also includes measurements of fracture surfaces, regarding orientation, roughness, fill, length and spacing. This can be both time consuming and can be at risk for the person performing the mapping. The amount of measurements can be insufficient and the environment is also dark, and only lit by the light from the drilling machine and a flashlight.

The LiDAR scanning system is a high resolution measurement system that enables a 3D model, and thereby enables mapping surfaces from blasted excavations and rock outcrop. In a relative short amount of time, it can give a representative picture of the scanned surface.

3.1 Instrumental characteristics

Terrestrial laser scanning, like LiDAR, enables the measurement and location of a large amount of data to be processed and shown as a 3D image of high resolution. One single laser scan can result in a point cloud consisting of tens of millions of points, and give information regarding its location in 3D, X, Y, Z coordinate system (Lato and Diederichs 2010). The laser scanners can measure the reflection intensity (i) of the target in sight. The intensity of the returned signal depends on the material of reflection, surface, and the angle of incident and the distance from the scanner to the survey points. This information is determined by the properties of the surface in mind, such as roughness or material type (Vassilis 2012).

LiDAR scanners measure the distance from the source to the target, either by time-of-flight or as a phase shift (Mechelke et al 2007). These two systems are used for different purpose, depending on the object in mind. The time of-flight scanner is used for scanning distances beyond 300 meters and has a scanning speed less than 4000 pts. /sec. Time-of-flight laser scanners emit a pulse of laser light that is reflected off the scanned object and sensors measures the time for the optical pulse to travel to and from the reflected surface. The mathematic formulae for the distance d to the object are given as (Vassilis 2012):

$$d = \frac{(c \times t\,)}{2}$$

where *c* is the speed of light and *t* is the flight time of light. The time it takes for a laser pulse to travel to the object surface and back is given by:

$$t = \frac{\theta}{2\pi \cdot f}$$

Where θ is the phase shift of the reflected wave compared to the emitted one and f is the modulation frequency of the wave.

In general, the main features that characterize a LiDAR system are: the maximum observation distance, the scanning speed, the phase shift and the measured quality in terms of precision, accuracy and repeatability. The laser beam is being deflected over a very accurate angular grid, and computes the coordinates for every measured point into an internal reference frame (Haugland 2010). The spherical coordinates are obtained by calculating the distance (d) to the reflecting object together with the horizontal (φ) and the vertical (α) angular component of the direction of the laser beam, as shown in figure on the next page.

The points are then converted in to the Cartesian coordinate system (x, y, z). All the points are measured relative to the scanner‘s position, which is defined as the origin $(0, 0, 0)$. In addition, the laser measures the intensity (i), based on the power of the reflected beam. The intensity from the back scattered signal depends on the moisture, color and roughness of the surface. The points

reflected to the scanner, consists of information of coordinates and intensity is resulting in a "point cloud" forming a highly visual 3D model of the surface scanned (Kemeny and Turner 2008).

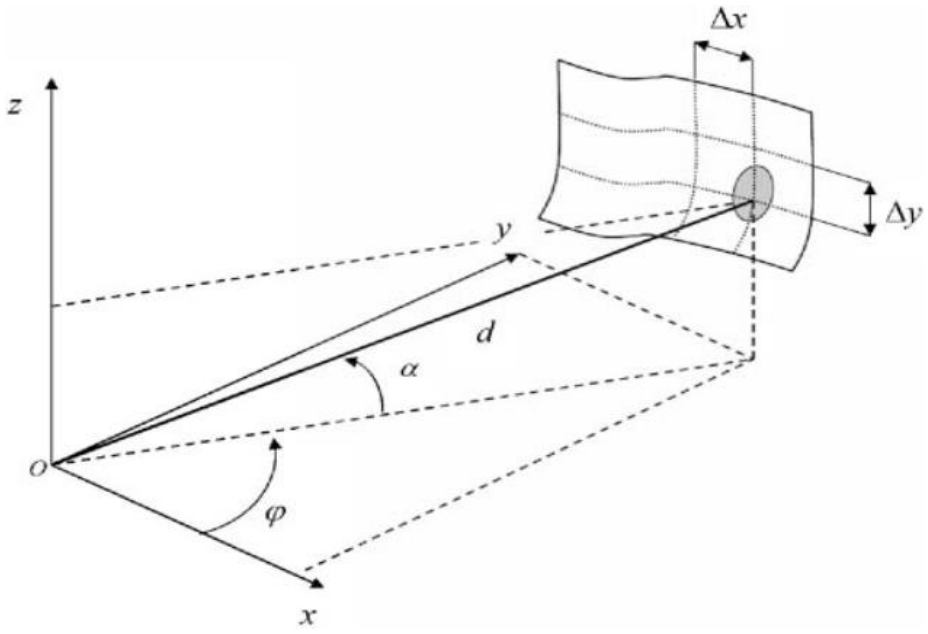

Figure 3-1: The principle of how LiDAR instruments determine the position in 3D space (Haugland 2010).

3.1.1 Density and resolution

The systems capability to collect information from the surface depends on the angle of incident between the scanner and the surface. As the angle of incident increases the probability to obtain satisfactory information in return decreases. Then as the scan density decreases the ability to visualize and delineate discontinuity surfaces decreases. One reason for this effect is the spot size and shape of the laser beam and the reflectivity of the object. The shape and its center position influence the reflection of the laser beam, which affects the precision of the scanned distance, and the 3D position of a scanned point within the point cloud. If the angle of incident is less than 45°, significant influence on the accuracy of the point cloud can be expected (Mechelke et al 2007).

The probability of joint detection, during virtual mapping, is also a direct function of the LiDAR point density within the visible joint surface (Lato and Diederichs 2010). The system‘s capability to reconstruct discontinuity surfaces also depends on the resolution as well as the quality of the triangulation process (Gigli and Casagli 2010). Depending on the type of scanner used, what type of object is scanned and the distance to the object, the resolution has to be determined. The scanners offer a range of resolutions with point clouds ranging from hundreds of thousands of point to tens of millions for a single scan (Fekete et al 2010). Depending on what type of laser scanner used, two kinds of resolution can be defined: Range resolution or angular resolution. The range resolution accounts for its ability to differentiate two objects on adjacent line-of-sight. This is governed by pulse length and typically is 3 to 4 mm for a long range instrument (Pesci et al 2011). The angular resolution is the ability to distinguish two different objects on the line of sight, and depends on spatial sampling interval and laser beam width and should lead to a corresponding spatial resolution of approximately 10 to 15 mm at 50 m distance (Pesci et al 2011).

An ideal scan resolution can be calculated from 86% of the beam diameter, depending on the properties of the laser beam. The beam diameter D will increase almost linearly with the distance d to the reflecting surface, and is described as:

$$D = a + bd$$

where a is the minimum beam diameter at exit and b is the beam divergence measured in radians (Haugland 2010). When the surface scanned is not perpendicular to the laser beam the surface diameter will increase. Pesci et al (2007) showed that for incidence angles greater than 60° the diameter increases dramatically with increasing range. Therefore, for more accurate point measurements it is recommended to scan the surface at a shorter range and a sharper angle of incidence.

When it comes to resolution, it is important to determine what kind of and how much information you require from a scan. When scanning with a high resolution, the sampling points will be many; you get a lot of unnecessary data. This will again lead to an excessive amount of time used on the processing of the data. But on the other side, when scanning with a small resolution, in-

formation can be missed and an accurate model of some features of the scanned object will be hard or even impossible to detect. Therefore, determining the resolution is of key importance.

3.2 Data collection with phase shift LiDAR

The LiDAR scanning system is set against a physical target or surface in mind and the laser beam is directed against the surface in a dense grid of points. By measuring the phase shift between the physical target and back to the scanner, the position in 3D space for each point will be created. This results in a point cloud, consisting thousands of 3D point that define a precise representation of the object. The data used in this thesis was converted, processed and analyzed in the commercial software PolyWorks.

The scanner which was used for collecting data for this thesis was a FARO Focus 3D scanner. It has distance accuracy up to ±2 mm; a range from 0, 6 up to 130 meters and it can measure up to 976, 000 points/sec. The scanner has a 360º horizontal field of view, and a 320º vertical field of view, scanning all but underneath the legs of the tripod setup. The scanner is mounted at a tripod on a relative flat surface, and must be completely steady during scanning. The best practice is to place the scanner is just inside the limit of supported rock, for human safety reasons and also for the risk of rock fall on the equipment during scanning.

The LiDAR data is not georeferenced to a global reference system; the collected scans will have separate coordinate systems and thus not align to each other when imported (Haugland 2010). This can be solved by placing reference targets in the scanners line of sight for each scan, scene establishing the location and orientation of the scanner, sighting back to known points. Reference point can easily be detected in the FARO Scene for alignment of multiple scans (FARO 2013). The scanner does not need to be leveled; however, leveling the scanner simplifies the scanner registration process (Haugland 2010).

The LiDAR scanner data collection requires about 4 – 6 minutes. This includes setting up, leveling the equipment, and scanning from one location. Faro Focus 3D has a built-in camera, so at the same time as the scanning takes place, high-resolution digital images can be taken. By knowing the position of the camera relative to the laser and the camera characteristics, a color point

cloud can be produced, and also the digital images can be draped onto the point cloud using texture-mapping techniques (FARO 2013).

The ability of the scanner to identify and measure the returned intensity is depended on the material, the angle of incident to the surface and objects in the line of sight. This requires that the dust from the blasting needs to be cleared and no sprayed concrete appliance during scanning. If the survey is of a complex structure with surfaces in several and varying orientations, it is recommended to perform two or three scans of the same surface. Shadow zones are referred to as occlusions and occur when parts of the rock surface cannot be sampled because of unfavorable orientations relative to the scanners line-of-sight (Lato and Diederichs 2010). This can give holes in the data sets. This is illustrated in figure 3-1. If the angle of incident between the laser beam and scanned surface is large, the amount of data returned is small. The scanner needs to be placed in a position so that all possible surfaces on the tunnel wall are being scanned and can give a return value back to the scanner. When analyzing discontinuity orientations from LiDAR data, the orientation relative to the scanners line of sight needs to be taken into consideration (Sturzenegger and Stead 2009). By scanning from two or three different locations at the tunnel face, occlusion and can be avoided and orientation bias can be reduced.

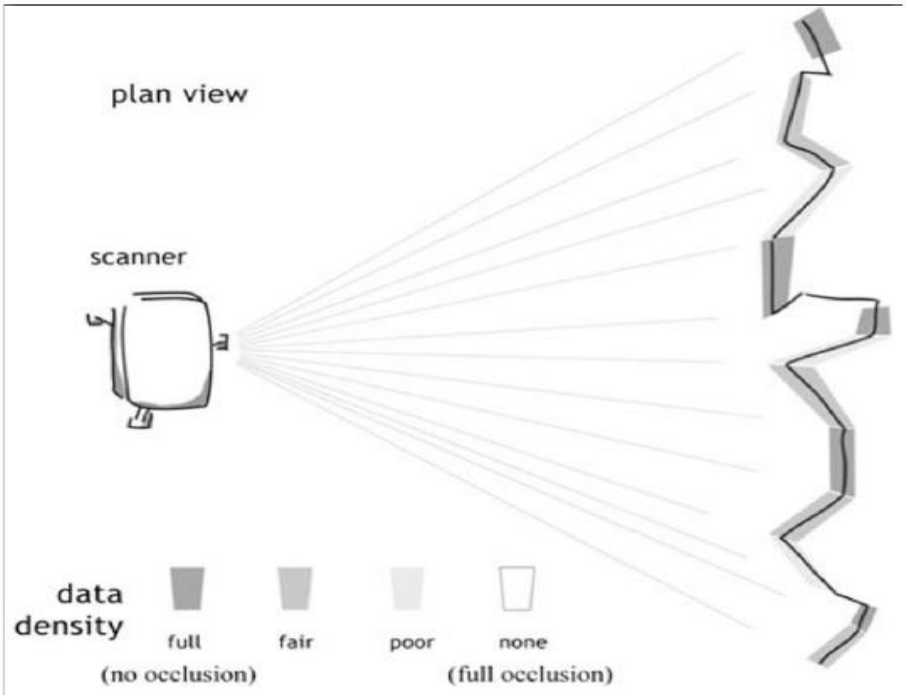

Figure 3-1: Visibility of fractures relative to the scanners line of sight. Surfaces not visible to the scanner or parallel to the scanners line of sight will result in full occlusion and as orientation bias respectively (Lato et al 2010).

3.3 Data processing in PolyWorks

After data capture the data should be processed. The point cloud collected contains accurate geometric information, and the data set needs processing. The processing involves reducing the size of the data set to a more manageable size, create continuous surface models and align the data with adjacent scans (Fekete et al 2010). The processing and analyzing of the data for this thesis is done in the commercial program PolyWorks version 11.0 13 (InnovMetric 2013). This is software which allows reverse-engineering and inspection applications by using the high density point cloud from the LiDAR scanning. A typical sequence of doing this is shown in figure 3-2.

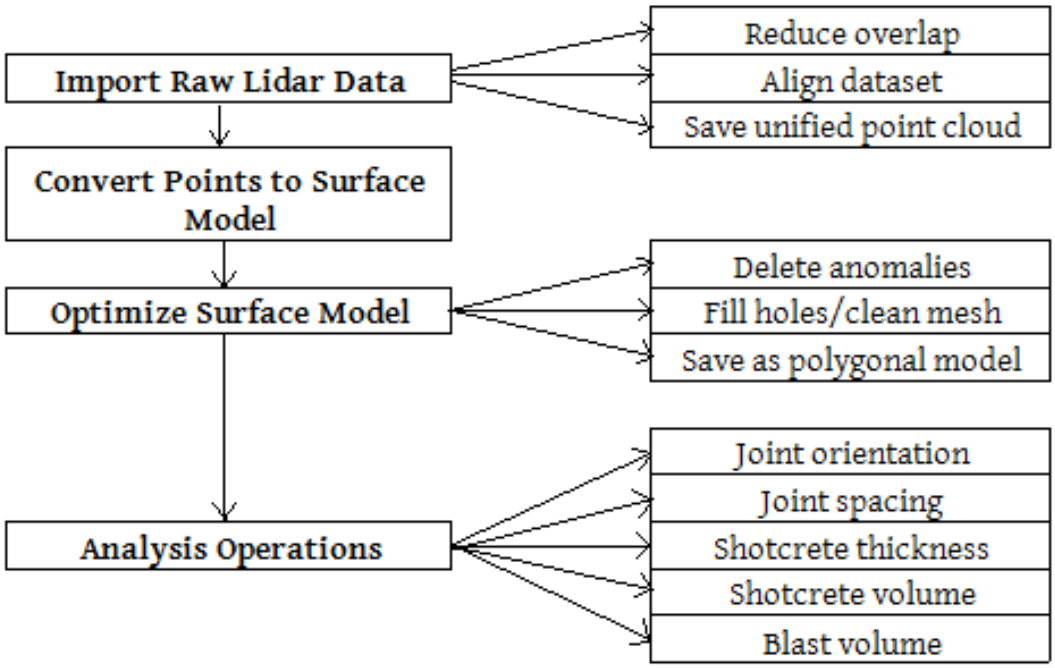

Figure 3-2: Processing work-flow for LiDAR data in PolyWorks (Morgan and Lato 2012).

3.3.1 Aligning the multiple point clouds

Aligning the data with adjacent scans is done to get a continuous model of all the scans performed of the tunnel. Each scan holds a lot of data, and to keep an efficient data processing, it is not recommended to align many scans at the same time. The alignment is done in the module IMAlign. It is done by selecting three or more common visible features in the point clouds, such as a morphological detail seen in the cavern or as a reference sphere. After rough matching the scans an interactive best fit alignment is run to fine tune the manual alignment. The coordinates of the selected points in the second scan is then aligned on the first scan, which is used as a reference (Pesci et al 2007).

After all the data sets are aligned together as a complete model, the surface in some areas can still have double sets of data. This could be due to inaccurate aligning or wrong parameter selection when running the alignment. Overlap reduction is performed to remove the overlapping or redundant data between the scans. Reducing this overlap is recommended prior to meshing due to the amount and size of data.

3.3.2 Meshing the point cloud

An important step in handling the large data sets and preparation for the analysis is the creation of the mesh or a surface model (Fekete et al 2010). This is not only for reducing the size of the data, but also to enable number of surveys and make assessment of fracture orientations. It is done by assigning groups of adjacent points lying on the same plane to triangles with a definite centroid, area, vertices and normal vector. The mesh often improves the interpreter‘s ability to visualize the data and required for any analysis requiring continuous surface information. After meshing the model can be visualized, analyzed and edited as wanted (Arayici 2007).

The meshing is performed in IMMerge in PolyWorks software. The meshing algorithm can automatically detect edges and fillets within a given radius range, and extract a theoretical line or surface to make the point cloud into a continuous model. This is done by triangulation of the point cloud, and making a mesh, where three vertices are contacted to form triangles which define the plane.

Meshing parameters like surface sampling step, reduce tolerance, smoothing and maximum distance are important to create a smooth and filtered high quality mesh model with high resolution. To accomplish this, the scanning parameters need to be taken in to consideration. The accuracy and resolution of the model will be depending on the accuracy and resolution of the laser scan. The first picture is of the point cloud, the second a triangulated mesh and the third the meshed tunnel model.

3.3.3 Editing the mesh – making a “watertight” model

After aligning and meshing the point cloud, the meshed point cloud is visualized as a complete 3D model. There may still be holes in the model due to imperfections in the point cloud. These holes can be effects of obstacles in the line of sight between the scanner and the surface or they may be due to occlusions, as discussed in chapter 3.2.
To make the model more watertight, an automatic algorithm in IMEdit is used. It has the ability do self-detect the holes and the function automatically fills the area. This depends on the settings for the algorithm. A maximum distance in the settings determines the size of the holes which should be filled. Holes with distance smaller than this are not filled. When the amount of data is

large and the maximum distance determined is relatively small, it can be time consuming. The uncertainties in the geometry and the size of the holes which should be filled can make the model imprecise and not give a realistic representation of the surface.

Although an automatic and manual filling algorithm is performed, the model can still contain holes. Choosing the Interactive Hole Filling button makes the holes that are not automatically filled to be highlighted. Then, by clicking on the highlighted areas the remaining holes will be filled.

The reason for making the model watertight is to make the line along the profile a continuous polyline, so that the length can be calculated. This is important to take in consideration when performing measurements at the model.

3.3.4 Orienting the tunnel axis with the y-axis orientation

For some inspection purposes of the point cloud, such as making cross sections and extract discontinuity measurements, the model needs to be set along a fixed axis. This can be done by changing the reference system by creating a cylinder feature to use as an axial reference system, so that the y- axis is parallel to the tunnel axis. Then the axis is moved a specific angle so that the tunnel axis is parallel to the true north.

4 Excavation and LiDAR scanning data at site

4.1 Location

The data used in this thesis is from the scanned surface of a water cavern in Nedre Romerike Vannverk, located close to Lillestrøm, Norway. The constructions of the cavern was executed in the period January to August 2011, and done by SKANSKA Norway. The facility consists of a 16.5 m long access tunnel, an about 17 m long cross over tunnel and a main cavern at about 232 m. The direction of the excavation is west to the east, and a plan view of the cavern is shown in yellow in figure 4-1.

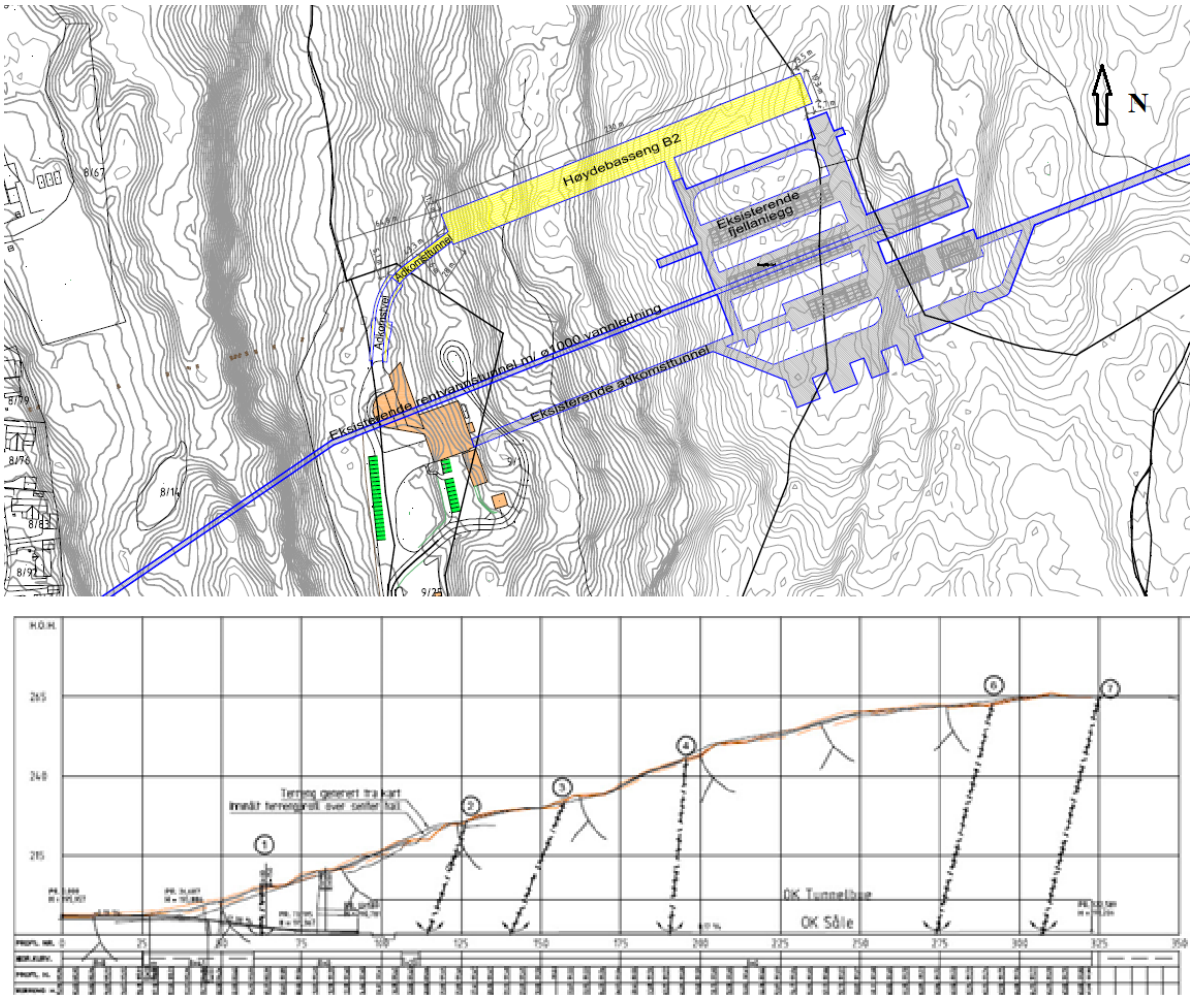

Figure 4-1: Location and longitudinal profile of the excavated cavern (Norwegian Geotechnical Institute 2013c)

4.2 Excavation and support

It is excavation consists of a cavern, access tunnel and a cross over tunnel, a total of approximately 45 000 m^3 rock (Morgan 2012). The 16,5 m long access tunnel has a cross sectional area approximately 55m^2, the 232 m long rock cavern has a span of about 19 m, with a cross sectional area about 170m^2, and the 17 m long crossover tunnel has a cross sectional area about 15 m^2. The height of the deflection in the main cavern is 3,5 m.

Because of the width of the main cavern, the excavation was divided in two, the pilot and the slash. The pilot was driven about 5-6 blasts in front of the slash and the length of each blasted round was normally between 4-6 m. The rock support was installed after each blasted round. The wall against the slash was not supported as it was blasted with the slash later. Because the cavern was excavated with a pilot 5-6 rounds in front of the slash, it was easier to predict the geology and hence the amount of support of the slash.

For determining the rock mass quality and permanent rock support, "the Norwegian method of tunneling" on the basis of the Q-method has been used. The rock mass quality of the main cavern has varied between Q = 0,8 in connection with weathered and altered zones, and Q = 25 in healthy mylonitic gneiss. The bolt pattern and bolt length in addition to the thickness of sprayed concrete for the permanent support was determined on the basis of the rock mass quality value.

As work support, CT bolts with dimension Φ = 20 mm, with lengths 3 m, 4 m, and 5 m and E700 fiber reinforced sprayed concrete were mainly used. As permanent support, the work support was supplemented with fully grouted bolts with dimension Φ = 20 mm, and lengths 6 m and 8 m. In addition, extra sprayed concrete was applied where the minimum thickness did not meet the requirements of the support. In two weakness zones in the cavern, profiles 134 – 141 and 195 – 210, reinforced sprayed concrete arches of the type E35/6 and E40/6 were installed (Morgan 2012).

The roughness factor used for determining the sprayed concrete volume was based on experience and the roughness factor used in the previous blasted round. By LiDAR control of the applied sprayed concrete it has been proven that the minimum thickness was not satisfactory and has led to further application later. The areas which needed more sprayed concrete were mapped out and handed over to the contractor for improvements.

4.3 Geological conditions

The geology in the area generally consists of basement rocks such as mica gneiss, pegmatite, migmatitic gneiss and also metatonalite. The metatonalite is often filled with small cavities. The rock mass showed varying degrees of altering, locally weathered and crushed to sugar cube sized fractions rock and also locally infected with swelling clay (Morgan 2012).

Three joint directions were mainly detected in the cavern. The main joint direction is N – S with a dip angle at 60º W, and the others have a fracture direction about N10ºE and N30ºE, both with dip angles 80ºE and 80ºW. In some areas between profiles 228 – 246 horizontal fractures were detected, giving the rock mass a flaky character. Generally the fracture directions gave rise to several block falls and wedge failures with dimensions up to $10m^3$.

30 minutes was set aside during construction to perform geological mapping of the surface. The mapping consisted of determining the Q-value, mapping the orientation and angles of the fractures and fractures and also scanning the tunnel surface with a LiDAR scanning system. The Figure 5-2 in chapter 5.1 shows the mapped surface done by the geologist at site.

4.4 LiDAR at site

After each blasted round, there were performed a scan of the cavern surface with LiDAR scanning system. Then after applying the sprayed concrete it was performed a new scan of the corresponding surface and it is these two surfaces which are being compared in this thesis.

Between the chainage no. 133 and 158, 2 scans for every blasted round were performed, between chainages no. 164 to 194; 1-2 scans and between chainages no. 291 and 325 1 scan for every blasted round was performed. The scans were processed in PolyWorks as described in Section 3.3.

5 Data analysis

This chapter will present and explain the methods used for comparison of the hand mapped data and the data from the scanned surfaces with LiDAR. It will also explain the method used for comparing the data of the scanned surfaces before and after applied sprayed concrete. In addition is has been done a correlation between the calculated roughness factors extracted from the comparison before and after sprayed concrete to geological features in the rock mass. This correlation was then used as a basis for a recommended look-up-chart.

When performing the comparison of the LiDAR data to the hand mapped data, the 3D model of the entire tunnel surface has been used. For the comparison of the surfaces before and after sprayed concrete the cavern has been divided into sections grouping together approximately similar values for the rock mass quality. The location of the cavern is provided in Figure 5-1. The size and dimensions are as described in section 4.2 and an overview of the separate sections is given in Table 5-1.

When a cavern surface is scanned with LiDAR a vast amount of data is generated. In addition the cavern is quite large and the data can be challenging and cumbersome to work with. Based on this it was determined to choose specific section for extraction of tunnel profiles. The sections with approximately uniform rock mass quality and type of geology were separated. In addition the tunnel is excavated with one pilot and one slash and therefore also the pilot and the slash are analyzed separately. The locations of these sections are visualized in Figure 5-1 and a description of the rock mass quality is listed in Table 5-2.

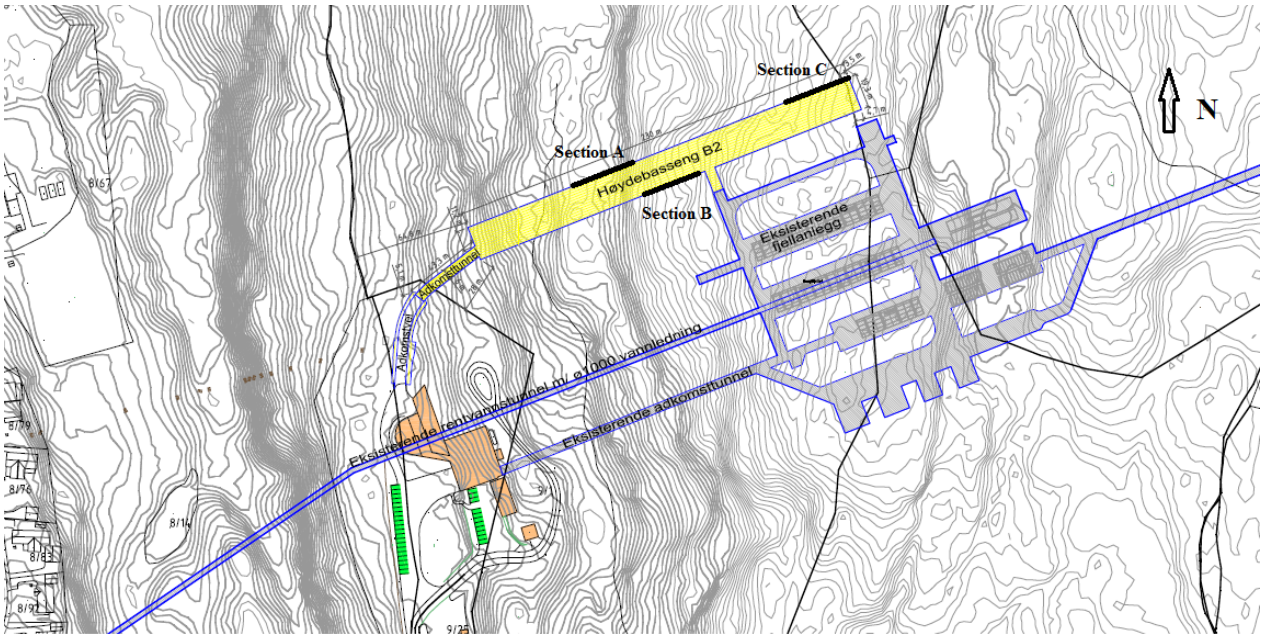

Figure 5-1: The Nedre Romerike Vannverk cavern. The location of the cavern (yellow) and the three sections where the profile analysis of the LiDAR data is performed, are marked as Section A, Section B and Section C in the figure (Modified from Morgan 2012)

Table 5-1: A description of the datasets used in the comparison. The datasets from the slash are given in the upper table and the datasets from the pilot are given in the lower table.

A: Datasets from the Pilot

Chainage number	No. of blasted rounds	Total length (m)	Average Rock Mass Class
79-122	10	44	C
126-159	7	31	E
164-194	7	30	C
199-213	4	14	E
218-228	3	10	D
233-248	4	15	D
253-268	4	16	C
273-325	11	52	C

B: Datasets from the Slash

Chainage number	No. of blasted rounds	Total length (m)	Average Rock Mass Class
79-123	10	44	D
128-159	7	31	E
164-194	7	30	C
199-213	4	14	E
217-227	3	10	C
232-247	4	15	E
253-269	4	16	D
273-325	11	52	B

Table 5-2: Description if the dataset used in the extraction of the roughness factor. The analyzed sections include both the pilot and the slash.

Section	Chainage number	No. of blasted rounds ana-lyzed	Total length (m)	Average Rock Mass Class	No. of Profiles
A	126-159	11	48	E	57
B	164-194	14	65	C	50
C	291-325	12	30	B	40

5.1 Comparison of the manually mapped data and the LiDAR scanned data

The advantage of the LiDAR data is its capability to permanently document the rock surface and conditions. This allows analysis and calculations after leaving the site and increases the ability to identify key discontinuity features and key failure modes. For this thesis it is of interest to use LiDAR data to recognize special features such as weakness zones, special characteristics when it comes to geometry and the rock mass quality. This is to assess the suitability of the use of LiDAR scanning system for further analysis of the rock surface.

5.1.1 Choosing a representative model of the scanned surface

For the data comparison and analysis, the commercial software PolyWorks Version 12.0.10 has been used. This is a tool for reverse engineering and inspection applications using a high-density point cloud. A geologist and engineer are able to view, process, and analyze the cloud data of underground excavations (InnovMetric 2013). The Workspace used in this task is IMInspect.

To work with the data set more efficient manner, the amount of active data displayed in the 3D-scene is reduced. The data is divided in to 7 sections with about 6 to 7 blasted round for each section. Also, ignoring or hiding the data not used in the analysis can make the data manageable in the 3D-scene, and save a lot of time.

One other important issue to consider is the “quality” of the data which should be analyzed. When processing the LiDAR data one must ensure that the alignment and the meshing of the point cloud is done in the best way possible. This provides an approximate watertight model of the meshed model and the model is giving a more representative image of the rock surface. These holes can to a certain extend be edited in IMEdit, but depending on the resolution of the mesh as discussed in chapter 3.1 and 3.3. The model used for this thesis has in some areas many holes. Because these areas does not visualize the true surface of the rock mass, these areas have to some extend been avoided.

5.1.2 Geological mapping conducted by the engineering geologist on site

Traditional mapping of the cavern surface by a geologist on site was performed after each blasted round. Rock mass classification was done by using the Q-method. Figure 5-1 gives an overview of the three selected areas which are used in the comparison and for extracting profiles for calculating the roughness factor. The areas inside the red markings represent three different types of rock mass quality and described in Section 4.3.

In the mapping form in Figure 5-2, the lines are given as joints and fractures along with its orientation. The grey areas are described as wedges and fall outs from the surface. The shaded square areas are not mapped.

The geology in Figure A represents very poor rock mass quality and consists of a weakness zone between the chainage no. 130 to 138. The general rock mass is partly crushed and severely transformed and brecciated, and the average Q-value lies between 1,5 to 1,8. The orientations of the main fractures are N10 Ø/80 V and in addition some less distinguished fractures with direction N30 Ø/80 Ø. The density of fracture sets increases, several rock falls in form of wedges from the roof have been registered. The size of these are usually 2 to 5 m^3. Chainage no. 141 to 145 was not mapped.

The middle picture (B) the rock mass quality is fair and less weathered than the previous section. The average Q-value is calculated to be between 5,8 to 6,1. The orientations of the fractures are the same, but the fractures with orientation N30 Ø/80 Ø are more prominent. The contents of clay and unsystematic orientation of the fractures has led to significant portion of loose blocks and unstable wedges in the roof. The size of the rock falls are about 10 m^3.

In the right hand figure (C) the rock mass quality is good and consists of unaltered gneiss. The rock mass is significantly less fractured and has some wide belts of pink pegmatite. There are in some places transverse fractures which contain increasing degree of mica minerals. The average calculated Q-value is between 9,6 and 19,9. The cross hatched region in this section has not been mapped.

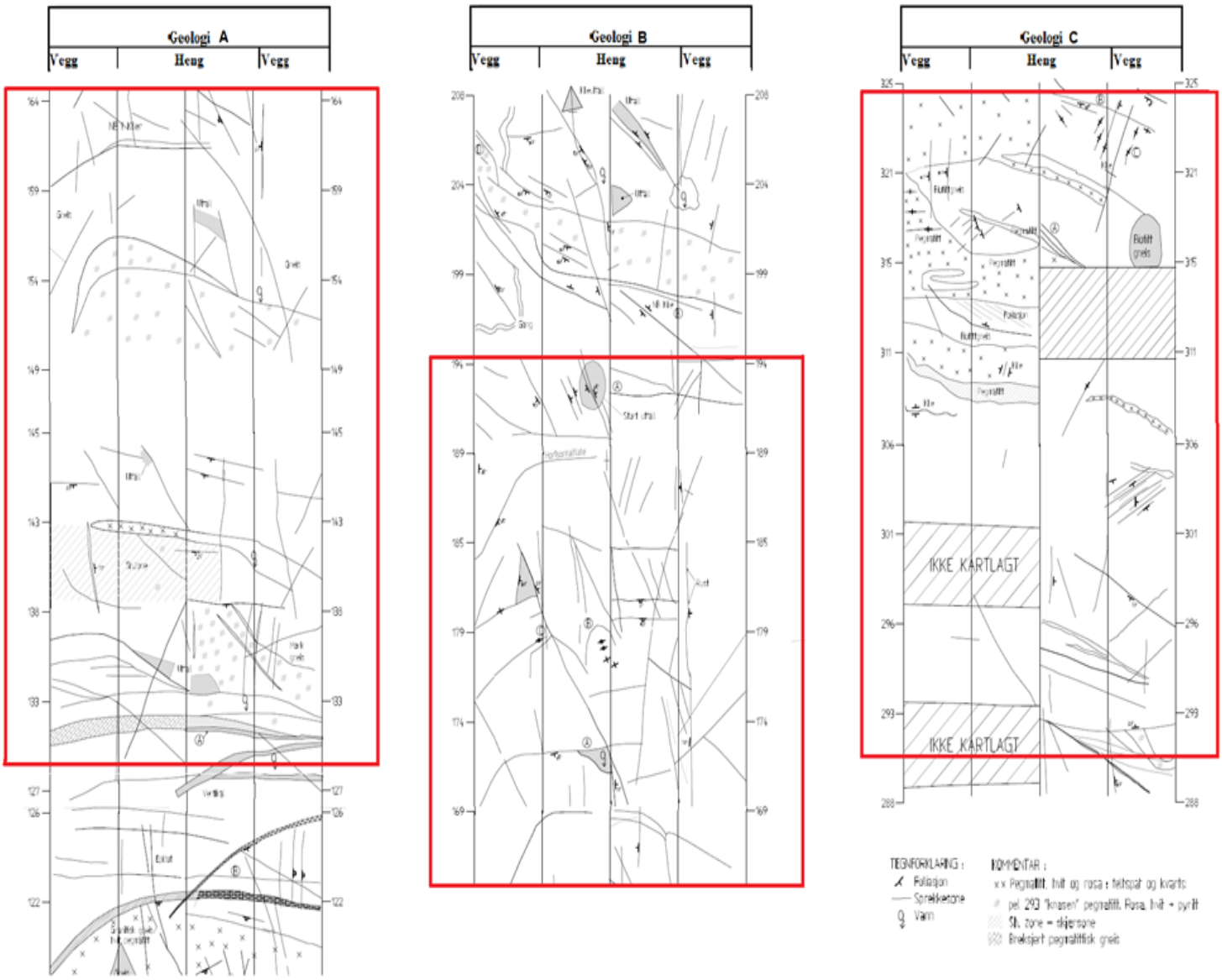

Figure 5-2: Geological mapping conducted by the engineering geologist on site. The three red markings represent the areas chosen for calculating the roughness factor. Geology A is between chainages no. 133-158, geology B is between chainages no.164-194 and Geology C is between chainages no. 291-325. The rock mass quality is very poor, poor and fair, respectively.

5.1.3 Comparing the manually mapped data and the LiDAR data

It is of interest to compare the LIDAR data to the corresponding sections of the hand mapped data. This is to assess the suitability of the use of LiDAR scanning system to recognize and visualize geological features in the rock surface. Features of most importance are weakness zones, special characteristics when it comes to geometry, geological structures and also an overall rock mass quality. This is performed to see if there may be a connection between the features and the roughness factor found later in this task.

5.2 Roughness analysis for sprayed concrete volume calculations

The method used today for extracting the volume of sprayed concrete in tunnel support is to use the theoretical volume of the tunnel excavation and multiply with a roughness factor. Extracting this roughness factor is based on experience and usually determined from the previous blasted round. This method can often be inaccurate and is non-scientific. Therefore it is a wish to establish methods for a more accurate determination of the roughness factor.

After every blasted round the amount of sprayed concrete is ordered from the producer. The volume needed to fulfill the minimum average thickness required must take into consider the roughness of the rock surface. The roughness factor takes into account the difference between the rough surfaces of the blasted rock compared to the smooth theoretical tunnel profile. The roughness factor in this thesis is extracted from dividing the profile lengths before and after applied sprayed concrete. This is done for every blasted round in the selected areas in the cavern.

5.2.1 Selecting areas of the tunnel surface for extraction of profiles

Due to the fact that the roughness factor for volume calculations is determined after every blasted round, an evaluation is done that the roughness factor calculated in this thesis should represent an average value of the roughness factor for the corresponding area. Therefore extracted profiles are measured for every blasted round. The total tunnel length is about 235 m, blasted as one pilot and one the slash leaving the total number of blasted rounds of about 90. Due to a time consuming method of measuring, the number of blasted rounds which were measured, was reduced and three sections for the extraction of profiles was selected. These three sections, shown in Figure 5-1and also described in Table 5-2, were selected as representative sections consists of

approximately uniform quality, fracture patterns and fracture orientation. Geology A, B and C consist of very poor, poor and fair rock mass quality, respectively.

5.2.2 Generating cross section for calculating roughness factor

The generating of cross sections is done in PolyWorks module IMInspect. Make sure that the data and the reference objects are displayed. This must be done so that all the surfaces which are being comparer are visible in the 2D view. The data which is not going to be used in the comparison can be hidden. This is to minimize the time it takes to generate the 3D scene and also minimize the profile processing time. In addition, when making cross sections, the program generates these sections perpendicular in to the model, so it is important to set the view in the –y direction, so that the tunnel is seen from above. Before making the cross sections, the model has to be aligned in the x, y and z direction as mentioned in Section 3.3.4.

The mapping of the tunnel surface and calculating the Q-value was done separately for the pilot and the slash. Because the pilot was excavated 5-6 rounds in front of the slash the amount of sprayed concrete was ordered separately. Due to this the pilot and the slash were analyzed separately and again each blasted round were analyzed separately. This leads to a generation of multiple profiles for the pilot and the slash separately and also for every blasted round. Multiple cross sections are made by choosing distance between each cross section and selecting a range. Cross sections were made for every 1 m and this produced between 5 and 7 cross section for each blasted round. Figure 5-3 shows the generated and measured cross section between chainages no. 144 to 155, from the pilot in the figure to the left and the slash in the figure to the right. In total it is produced approximately 190 profiles but due to holes and other irregularities discussed in the next section, only 147 profiles have been used.

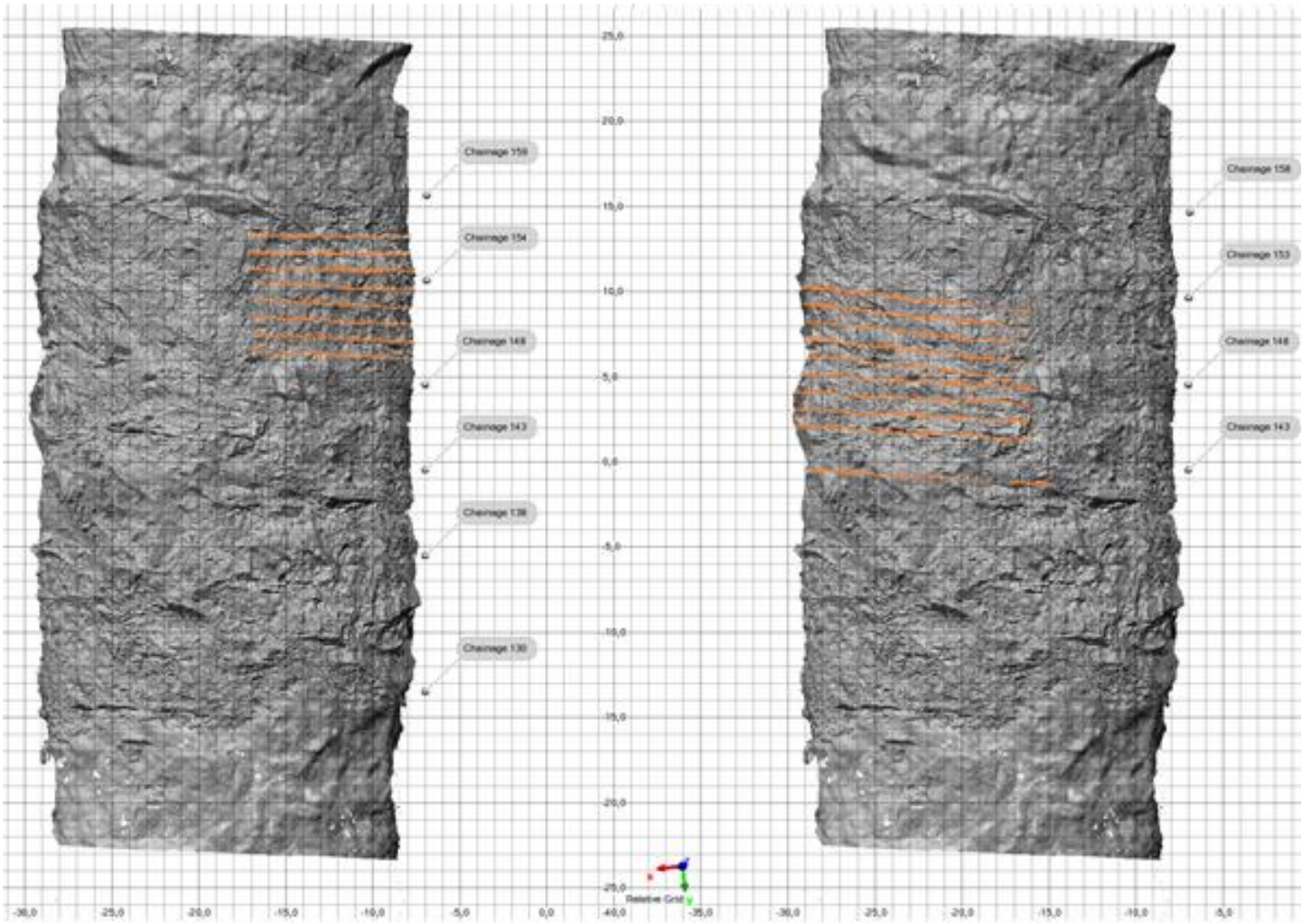

Figure 5-3: A 3D model of Chainages between 138 and 158, seen form above. Multiple cross sections generated at the pilot in the figure to the left, and likewise at the slash in the figure to the right.

5.2.3 Measuring the profile lengths

The cross sections are generated in the 3D scene in the z-direction and each cross section is viewed in the 2D view in the IMInspect module. The cross sections are seen in the y-direction, which is perpendicular to the generated cross section and along the tunnel axis. The lines in the generated cross sections represent the rock surface and the sprayed concrete surface. The sprayed concrete was applied from the tunnel crown and to 2 m above the floor. The measurements of the

profiles therefore excluded the two bottom meters of the wall, the tunnel floor and the wall between the pilot and the slash.

The scan of the surface was done after each blasted round by a geologist on site. The new scan also includes data from the previous blasted round in addition to the recently blasted surface. Between these blastings, several cases of rock fall occurred from the roof. By scanning the same surface before and after a rock falls, the meshed model can get a double set of data, as visualized in the picture to the right top in Figure 5-4. These are also shown as grey areas in the 3D model or they have the same color as the sprayed concrete in the model. It is in some cases difficult to decide if these areas give a representative image of the true rock or sprayed concrete surface and therefore these areas has been tried to been avoided in the analysis. Cross sections with multiple lines, as shown in the Figure 5-4 left top and bottom, are excluded from the analysis due to difficulties finding the true line representing the rock surface.

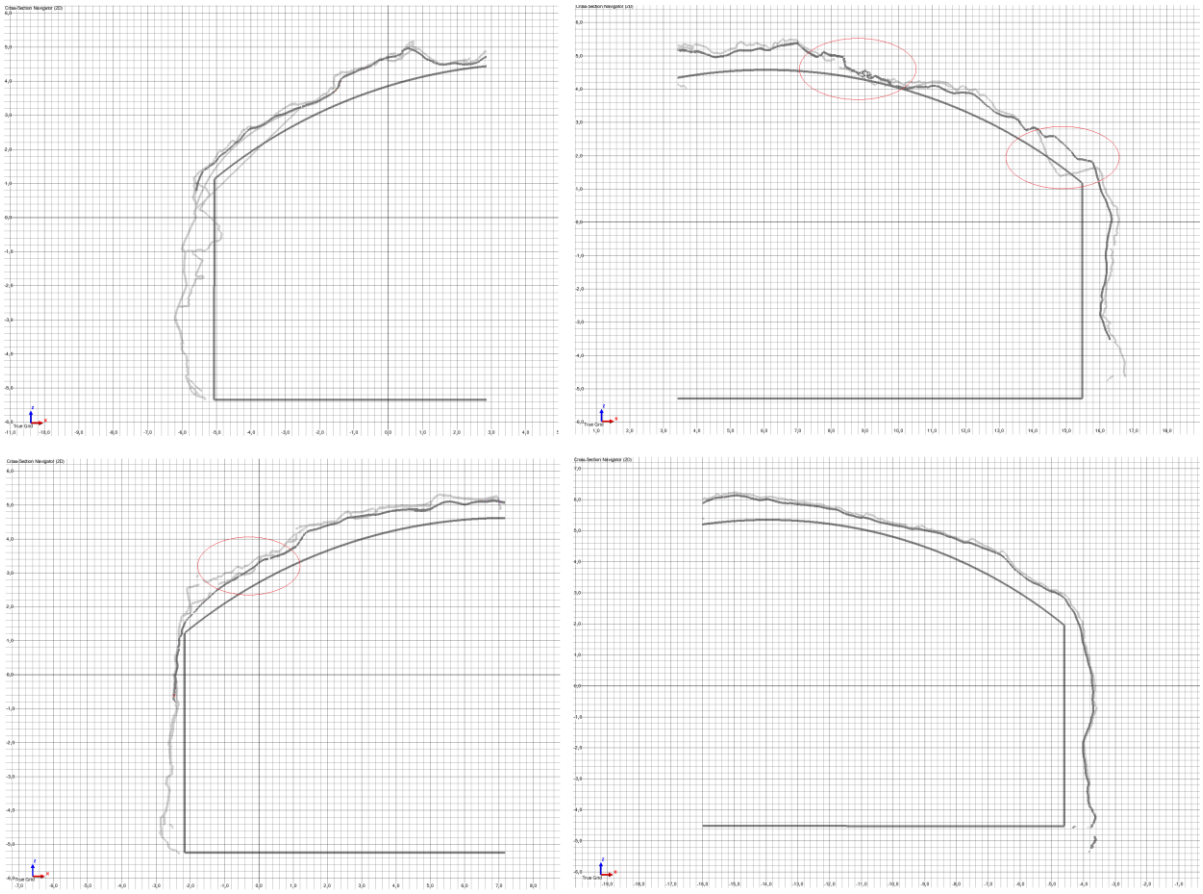

Figure 5-4: Profiles showing different types of cross sections from the analysis. Top left shows multiple lengths, top right shows fall outs from the roof between scans, bottom left shows discontinuous lines, and bottom right shows a continuous and representative profile.

In order to take measurements of the cross section it is important that the model is as watertight as possible, as discussed in the previous chapter. Watertight meshed models generate continuous lines in the cross sections and when measuring the length, it is necessary that the line representing the surface is as continuous as possible. Some holes can still occur in the model even if the model is aligned, meshed and edited well. The model used in this thesis was not completely watertight and some areas consisted of several small holes. This led to non-continuous lines representing the rock surface cross section and the sprayed concrete surface cross section. Measuring the cross section was done by clicking on the lines, along the profile, from one end to the other. Holes in the non-continuous line were not measured. The lengths were exported in to Excel and summarized. The left picture in Figure 5-5 shows a profile which has continuous polylines

leaving the small holes in between the lines to a minimum. The picture to the right has several short polylines. This may lead to imprecise measuring and the chance of error in the total measured length is high.

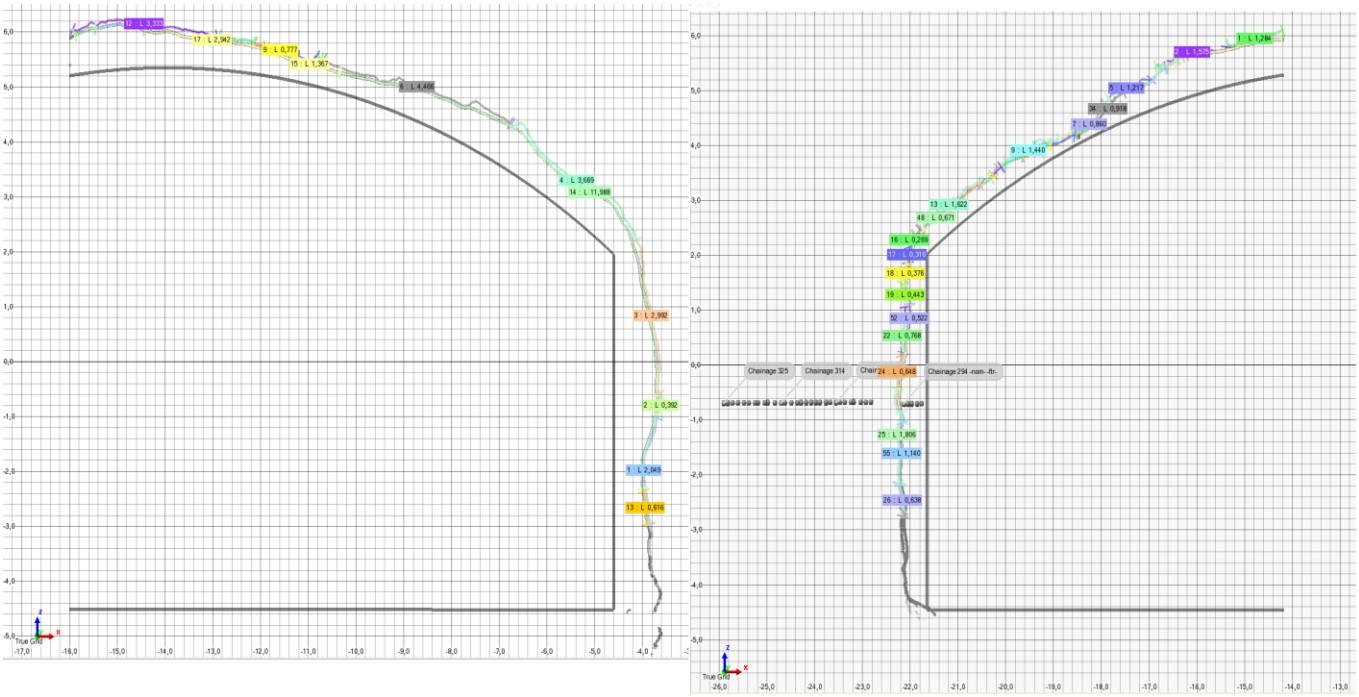

Figure 5-5: Measured cross section lengths, showing only about 15 measured lengths along the cross section in the picture to the left, and to the right showing about 80 measured lengths along the cross section.

5.2.4 Calculating the average roughness factor using cross section lengths

The roughness factor in tunneling is the relationship between the actual blasted surface and the theoretical blasted surface. This roughness factor needs to take in to account the varying rock mass condition and the minimum required thickness of applied sprayed concrete. The roughness factor calculated in this thesis is the relationship between the actual blasted surface and the surface of the sprayed concrete.

Because the roughness factor is determined for every blasted round the cross section length roughness factor is calculated for each blasted round. This is done by measuring 3 to 7 profiles

for every blasted round and then calculated the average roughness factor for the surface. This method is chosen because it is assumed that this gives the most representative roughness factor for the hole blasted round. It was considered to summarize all the cross section lengths of the rock mass surface and divide the summarized lengths for the sprayed concrete, but since the lengths for every cross section are highly variable, it would not give a true roughness factor for the blasted round.

5.3 Develop methodologies for estimation of the roughness factor

It is a goal to develop methodologies for a more accurate determination of this factor by using the LiDAR scanning data. The goal of this thesis is to find parameters which may be of importance when determining the roughness factor in tunnels. Therefore several correlations have been done to see if and which parameters that can have an impact on the surface roughness.

After every blasted round the average Q-value for the blasted area is determined. Also, the roughness factor is as mentioned "determined" after every blasted round. It is therefore of interest to examine if it is a correlation with these two values. The study includes evaluation of the correlation with the Q-value, the RQD/J_n quotient, the RQD value and the joint set number J_n.

Three sections were analyzed. The reason for choosing these three sections was because they were representative for geological conditions in other sections of the cavern. This was done by calculating the average roughness factor for every rock mass quality class within the analyzed areas and these values were compared to the corresponding basted rounds with same rock mass quality.

5.3.1 Correlation between the calculated roughness factor and the Q-value

It is a future goal to incorporate a recommended roughness factor in to the Q-chart. The Q-chart recommends that the thickness of the applied sprayed concrete should increase with decreasing Q-value. It is a goal to see if correlations can be made between the estimated roughness factor from this analysis and the Q-value for the same area.

5.3.2 Correlation between the calculated roughness factor and the RQD / J_n parameter

The Q-value consists of three quotients mentioned in Section 2-2. The quotients represent different qualities and properties for the rock mass. The two last quotients represent qualities

anticipated not to be of significance to this analysis and are therefore not included in this analysis. The first quotient RQD/J_n, relates to the structure of the rock mass giving a measurement of the relative block size in rock mass. An assumption is made that this may have an impact on the roughness of the tunnel surface and therefore an evaluation of the correlation between the calculated roughness factor and the RQD/ J_n is performed.

5.3.3 Correlation between the calculated roughness factor and Rock Quality Designation (RQD)

The structure of the rock has an impact on the amount of rock support required. An assumption is made that the amount of sprayed concrete used increases with increasing degree of joints and fractures. A measure for the degree of jointing or block size is the rock quality designation (RQD) factor. An evaluation of the correlation between the roughness factor and the RQD parameter in the Q-value has therefore been performed.

5.3.4 Correlation between the calculated roughness factor and the joint set number (J_n)

The joint set number $J_n$is not necessarily a typical indicator for highly and fractured or poor rock mass quality. A rock mass consisting of a few fractures may still be of poor or very poor quality. It is still anticipated that J_n may influence the roughness of the rock mass surface. Therefore an analysis of the correlation between the calculated roughness factor and the joint set number is conducted.

5.3.5 Calculated roughness factor in weakness zones and wedges

The presence of weakness zones can have a large impact on the stability of the rock mass in tunnels. They may consist of very crushed and brecciated rock mass and often swelling clays and water are present. The support of weakness zones is often performed by using ribs of sprayed concrete and the amount of sprayed concrete may be significantly increased in these areas. Therefore it is a goal to investigate if there is a connection between the calculated roughness factor and the geology in the weakness zones in the cavern.

The structure of the rock can have an impact on the formation of blocks and wedges in the tunnel surface. The presence of wedges is strongly connected with the joint set number but differs in terms of the orientation of the fractures. While the joint set number only consider the number of

fractures, wedges appear where the orientation is unfavorable relative to the orientation of the tunnel. The detection of wedges in the 3D model is described in Section 5-1.

5.3.6 Calculated roughness factors in cross sections with small scale an large scale roughness or a combination of these two

Factors affecting the roughness of a tunnel surface and cross section depend on the geology and how the blasting is executed. Large scale roughness may be caused by larger rock falls or wedges and can be visualized as large irregularities of the tunnel surface or the cross section line. Small scale roughness is characterized as pebbled and a large grade of unevenness may be present.

Extracting representative cross sections of the surface roughness is done by visualizing and studying the cross sections generated in PolyWorks. Cross sections showing both large scale and small scale roughness typically consist of rock fall or wedges from the tunnel surface, either from the roof or the wall. It must be mentioned that the description of the roughness of the tunnel surface for the selected cross sections must be seen relative to the rest of the tunnel cross sections.

Based on the chosen cross sections representing the different types of roughness a correlation is done between the calculated roughness factor and small scale roughness, large scale roughness and a combination of these two.

5.4 Creating and calibrating a look-up-chart for estimating the roughness factor in tunnel applications

For the calculation of the roughness factor the true cross section of the rock masses should be used and not the theoretical surface. Analyses are done in this thesis to establish a method for a more precise method for determining the roughness factor for tunnel applications. It is a goal to create and calibrate a look-up-chart that will enable the engineer and contractor to better estimate the roughness factor when calculating the required sprayed concrete volume. This may be done by analyzing the LiDAR model for the tunnel to find parameters of importance for better determining the roughness factor.

5.4.1 Selecting the parameters for determining the roughness factor

The traditional determination of the roughness factor usually takes place after each blasted round. The roughness factor depends on the geology, fracture orientation and how well the rock mass has been blasted. This can often be difficult to determine until the rock surface is visible and can be studied by an engineering geologist on site. By calibrating a look-up-chart taking all these factors in to account determination of the roughness factor may be more precisely.

5.4.2 Selecting values and boundaries

The determination of the roughness factor has previous been based on an assumption that the Q-value can have an influence on the roughness factor. Based on this it is therefore decided to create a look-up-chart or that the results can be incorporated in the Q-system in some way. Depending on the results from the correlation of the calculated roughness factor and the Q-value, may this result also verify the assumption.

Creating and calibrating a look-up-chart require development of values and boundaries. The values will be determined based on the results from the comparison and the calculations of the roughness factors in Section 5.2. The boundaries are selected form correlation of the calculated roughness factor and Q-value together with other important geological factors decided in the results.

.

6 Results

This chapter will present the results of the analyses described in Chapter 5. Presented first is the result from the comparison of the hand mapped data conducted by the engineering geologist on site with the LiDAR data of the corresponding section. Secondly, the calculated roughness factors from the measured profile lengths are given and also a presentation of the relationships that may affect the determination of the roughness factor for tunneling applications. Finally, an assessment and recommendations of values and boundaries for the look-up-chart are provided.

6.1 Comparing geological features in manually mapped data with the LiDAR data

This section will present the results from the comparisons of the hand mapped data to the corresponding sections of the LiDAR scanning data. This is to assess the suitability of the use of the LiDAR scanning system to recognize and visualize geological features in the rock surface. These features are known structures, wedges and weakness zones detected by the engineering geologist on site and described in the hand mapped data.

6.1.1 Detection of major structures and geometry

The 3D model depends on the parameters used on the scanner, especially the intensity value (i) reflected from the rock surface to the scanner. The intensity value enables differentiation between materials of different reflectivity in the LiDAR data.

Pegmatitic dikes are not easily detected in the LiDAR data. The general geology in the tunnel is as described earlier metamorphic rock, and in some places belts of pink pegmatite appear with different orientation than the rest of the rock mass. The belts are drawn in the hand mapped data and a photo of the belts is taken by engineering geologist on site. The photo can be seen in the picture to the right in Figure 6-1 and an image of the 3D model of the same area is provided. In the LiDAR data it is difficult to recognize the same structures. You have to know that there is a belt there to be able to “see” the structure in the model. The difficulties with seeing the structure may be due to that the belts are so narrow and may also have the same intensities than the sur-

rounding rock mass. The surface of the belt can also be rough and the model does differentiate between the pegmatite and the surrounding rock mass.

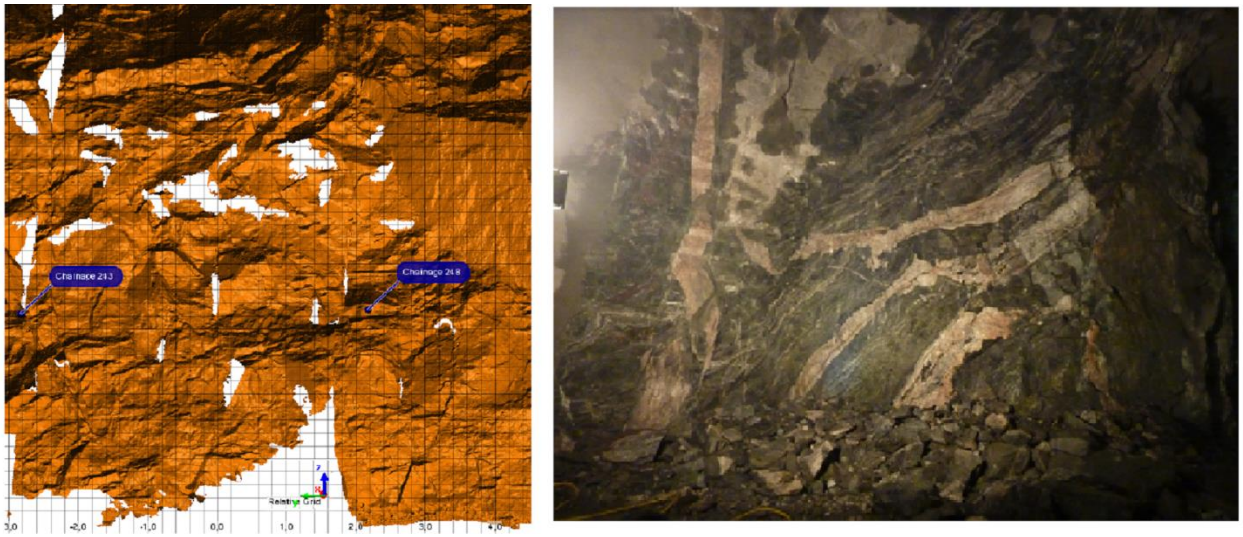

Figure 6-1: a) Picture of the same surface of the rock mass of the wall at the slash near Chainage 242. b) An image of the 3D model generated from LiDAR data to the left and photograph taken by the engineering geologist on site to the right and

Although belts are not detected, the wedges are possible to detect in the 3D model. In the 3D model it is easy to detect the different planes that constitute the wedges and the dip and dip direction. In Figure 6-2 the same section of the rock surface is displayed, with LiDAR to the left and hand mapped data to the right. Fractures with almost the same dip direction but different dip angle run from the roof at Chainage 169 and extends obliquely to the left side at Chainage 185. The orientation of the fracture surfaces makes two distinguished wedges in the tunnel roof. This can be seen in the image generated by the 3D model in Figure 6-2 a). Other fractures and fractures are also visualized in the 3D picture. Due to the inaccuracy in measuring and drawing by hand the hand mapped data may differ slightly in place and direction from the LiDAR model.

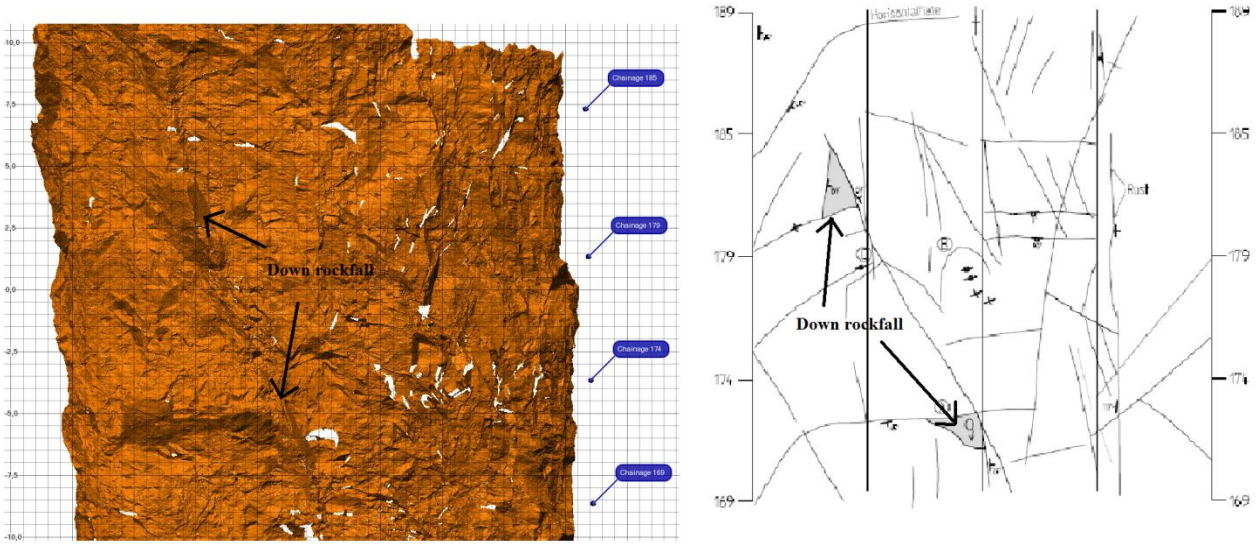

Figure 6-2: a) Image of the 3D model from the chainages no. 169 to 185 seen from above. A wedge running from the middle of the roof at chainage no. 169 and continues obliquely towards the slash. b) The manually mapped data of the same section and the grey areas represent the wedge fall outs.

From the hand mapped data it is detected rock falls from the roof in two different sections. The volumes of these wedges are calculated to be approximately 5 to 10m^2, and are primarily due to the orientation of the main fracture sets together with other unsystematic fracture systems. The analysis is also done for chainages no. 127 to 148 and confirms the same as described here.

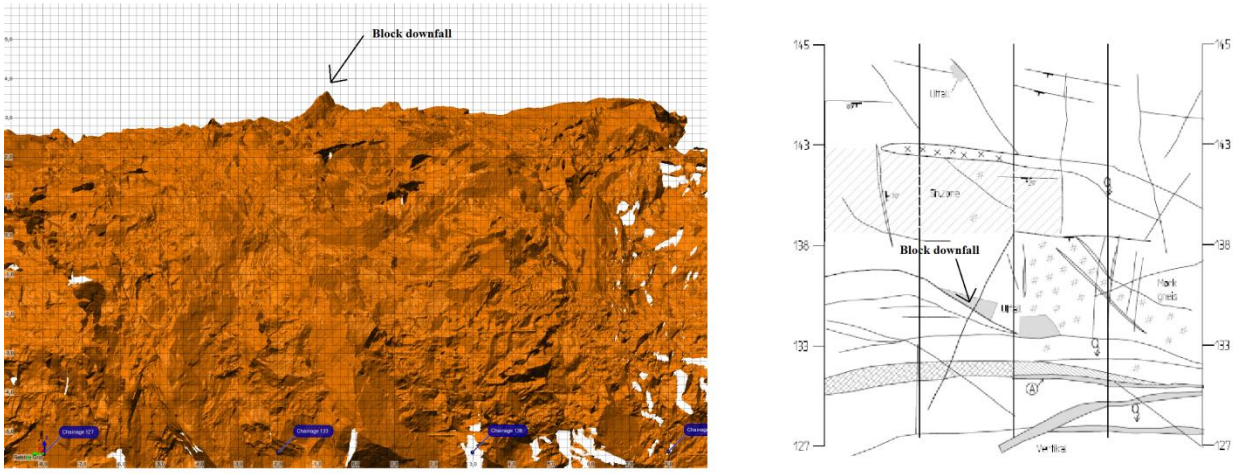

Figure 6-3: a) Image of the 3D model from the chainages no. 127 to 148 seen from the side. b) The manually drawn mapped data of the same wedge seen from above.

6.1.2 Recognizing weakness zones

From the hand mapped data it is detected two shear zones in the tunnel. These two zones are between the chainages no. 138-143 and 199-206. The rock mass quality is very poor and it has been detected several rock falls at about 5 m^3during excavation from both weakness zones.

Figure 6-4 a) and b) are LiDAR models of the rock surface in these two zones. In picture 6-4 a) it is an image generated from the 3D model of the rock surfaces, intending to visualize the weakness zone between chainage no. 138 to 143, while picture 6-3 b) displays the weakness zone between chainage no. 199 to 206. From the pictures it can be difficult to detect the weakness zones in the LiDAR model. The surrounding rock mass seem to have the same structure as the rock mass in the weakness zone. The rock mass are very crushed and brecciated, so it is difficult to decide whether there is a weakness zone present or not. The general feature of the section is that the geology seems to have the same type of blockyness or small scale roughness. At the the slash side of the tunnel by chainage no. 206 some rock falls from the roof of the tunnel can be seen. It is difficult to determine whether the rock fall is due to the geometry of the tunnel, poor blasting or with the weakness zone itself. A general characteristic of the weakness zones is that the rock mass generally is crushed and consists of large amount of a small scale roughness.

The LiDAR data cannot detect the quality, in example a Q-value, in the rock mass. On the other hand, it can visualize how crushed the rock mass is. It is possible to see how a rock mass is crushed relative to the nearby rock masses. Crushed rock mass was detected especially in areas near the weakness zones.

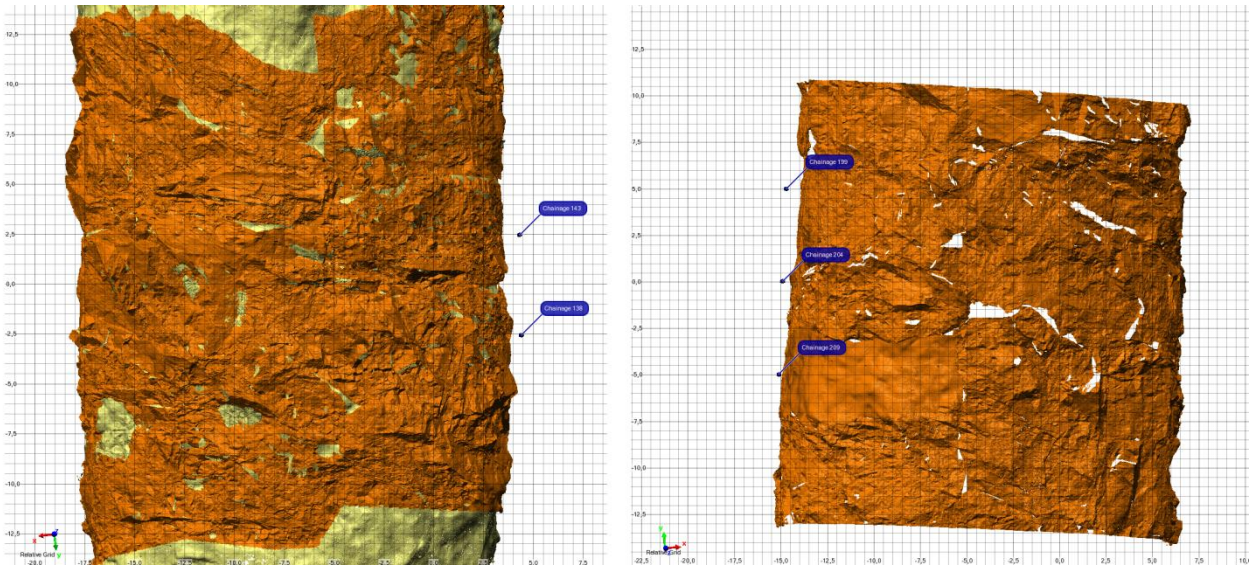

Figure 6-4: A 3D image of the weakness zones seen from above. a) Weakness zone between chainage no. 134 to 143. b) Weakness zone between chainage no. 199 to 206.

6.2 Calculated roughness factor from applied sprayed concrete volume

This section presents the results from the analysis described in Section 5-2 using LiDAR data for estimating a roughness factor for applied sprayed concrete. An average roughness factor has been calculated for the selected blasted rounds. Due to a very time consuming process it was necessary to reduce the amount of profiles analyzed and divide the cavern in to smaller sections with uniform and similar rock mass quality.

6.2.1 Calculated roughness factor using profile length

The length of the rock surface is divided by length of the sprayed concrete surface for calculation of the roughness factor. Table 6-1 shows the results of the comparison. Also extended tables of

the measured lengths of the profiles are provided in tables A-1, A-2 and A-3 in Appendix A. The roughness factor presented is based on the average roughness factor for every blasted round and is calculated by taking the relationship between the blasted surface and the same surface after sprayed concrete.

As seen from the results presented in Table 6-1 the trend is that the roughness factor is larger for Geology A, which consists of very poor rock mass quality and smaller for Geology C, which is of fair rock mass quality. The roughness factor for Geology B lies in between the roughness factor for Geology A and Geology C.

The roughness factor in Table 6-1 is calculated in order to see if there is a correlation between the roughness factor and the all-round structure and quality of the rock mass. By visually studying the 3D models of the three sections of Geology A, B and C, and the roughness factors presented in the table, it can be seen that the roughness factor appears to have correlation with the rough nature of the rock mass. Geology A represents the roughest surface and mainly small scale roughness. It is believed that an increasing degree of small scale roughness increases the area of the surface and hence gives a larger profile length, which again leads to a larger roughness factor. In addition it has been some rock falls from the roof and this also increases the profile length of the rock surface. The average roughness factors for the pilot and the slash and its geology are also presented in Table 6-2. The roughness factors calculated for Geology B is lower than for Geology A. The surface of the section is smoother and thus gives a smaller roughness factor. For Geology C the roughness factor is the smallest.

Table 6-1: Results from the calculation of the roughness factor for Geology A, Geology B and Geology C, and also divided in pilot and the slash. The results are extended from the profiles in the 3D model.

	Chainage no. The slash	Roughness factor	Chainage no. Pilot	Roughness factor
Geology A	133	**1,08**	130	**1,14**
	135	**1,16**	138	**1,15**
	143	**1,09**	143	**1,16**
	148	**1,11**	148	**1,08**
	153	**1,11**	154	**1,14**
	158	**1,14**	159	**1,18**
Geology B	164	**1,08**	164	**1,12**
	169	**1,08**	169	**1,10**
	174	**1,09**	174	**1,09**
	179	**1,09**	179	**1,07**
	185	**1,06**	184	**1,10**
	189	**1,07**	189	**1,10**
	194	**1,06**	194	**1,13**
Geology C	291	No rock data	291	**1,07**
	298	**1,06**	296	**1,04**
	304	No rock data	301	**1,07**
	310	**1,04**	306	**1,07**
	315	**1,04**	311	**1,04**
	320	**1,04**	321	**1,07**
	325	**1,02**	325	**1,06**

Table 6-2: Table of the average calculated roughness factors for Geology A, Geology B and Geology C, also divided into Pilot and Slash.

	Chainage no. Slash	Roughness factor	Chainage no. Pilot	Roughness factor
Geology A	133-158	**1,12**	130-159	**1,14**
Geology B	164-194	**1,08**	164-194	**1,11**
Geology C	291-325	**1,04**	291-235	**1,06**

In addition to the difference between the different types of geologies, it is also a difference between the pilot and the slash for the approximately same chainage number. The reason may be that the main crack direction is lying angled relative to the direction of the orientation of the cavern. This causes a shift in the rock mass quality and hence the roughness factor for the same chainages. It can also be registered that the roughness factor is generally larger for the slash than the pilot. This may be caused by unfavorable crack orientation and rock falls which are more prominent in the slash than in the pilot.

6.3 Develop methodologies for estimating the roughness factor

This section presents the results from the analysis described in Section 5-3 of comparing the calculated roughness factor to geological features. First presented are the results of the correlation between the roughness factor and the Q-value, and also its quotients and parameters. Secondly the correlation between the roughness factor and weakness zones are performed and the presence of wedges. At last it is done a correlation with different types of roughness scale.

6.3.1 Roughness factor and the Q-value

The aim is to see if there exists a correlation between the roughness factor estimated in this thesis and the Q-value of the rock mass. Due to the amount of data it is made an assumption that sections which are not analyzed can be assigned the same roughness factor as the analyzed sections with the corresponding rock mass quality. This means that the mean value of the roughness factor should be representative for other areas of similar rock mass quality. The calculated and the suggested values are given in table 6-3 below.

Table 6-3: Table showing the estimated roughness factor for a number of blasted rounds analyzed for a given rock mass quality.

Rock Mass Quality	No. Of blasted rounds analyzed	Average roughness factor
E	6	1,13
D	8	1,11
C	16	1,08
B	7	1,05

The calculated average roughness factor is compared to the Q-value for the corresponding sections. Figure 6-4 shows the result of the comparison. The vertical scale represents the calculated roughness factors and the horizontal scale represents the Q-values in a logarithmic scale.

From the figure it can be interpreted that the roughness factor can have a correlation with the Q-value. The results suggest that the roughness factor decreases with increasing rock mass quality. This is also suggested from Table 6-1 above. Even though these results indicate a trend it must be pointed out that for some Q-values the interval of the roughness factor can be quite large. For a Q-value of 7-8 it can be seen values of the roughness factor range from about 1,04 to 1,14 and also for Q-values 3-4 a roughness factor from about 1.08 to 1.18 . The span and variation of the roughness values indicate some difference in the calculated roughness factors for the same value of rock mass quality.

The marking with roughness factor 1,18 at rock mass quality approximately 2,3 differs somewhat from the rest of the calculated values. This is due to a large rock fall from the roof in this area, and the calculated roughness factors for some profiles were around 1,22, making the average roughness factor very high for that blasted round.

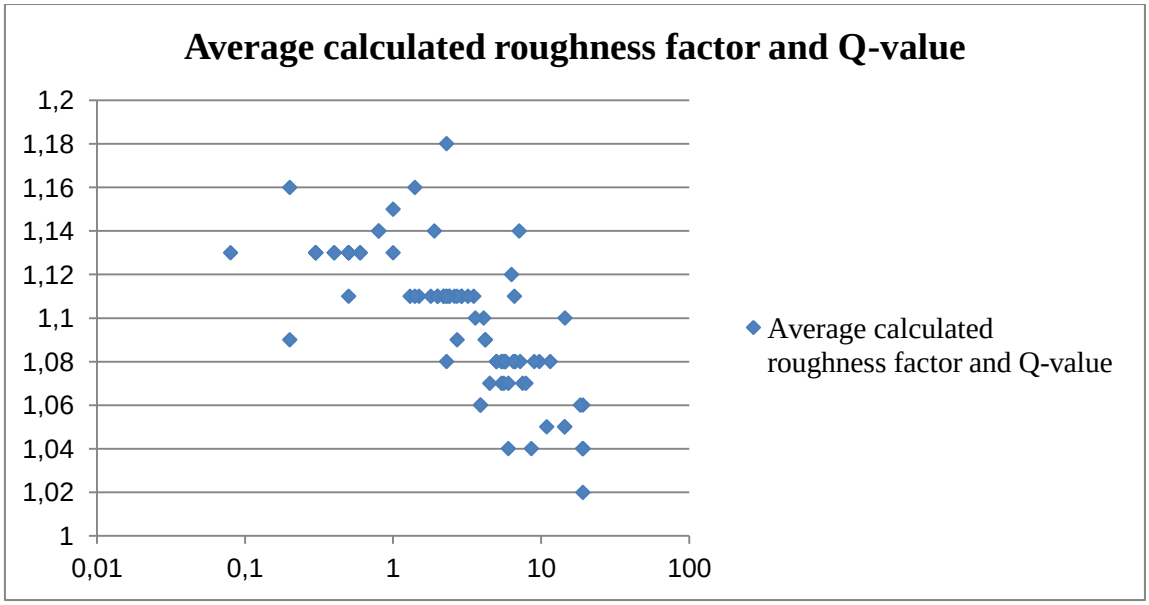

Figure 6-4: Plot of the average calculated roughness factor and the Q-value. Note that the scale of the Q- value is logarithmic.

6.3.2 Roughness factor and the RQD / J_n quotient

The calculated roughness factor has been correlated with the RQD / J_n quotient in the Q-system. This is done to evaluate if the overall structure of the rock mass can be used for describing the roughness of the tunnel surface. Figure 6-5 below shows the results of the correlation.

As seen from the plot in Figure 6-5, a certain degree of correlation is shown, but it is no obvious trend. The value of the roughness factor can vary up to 0,10 for certain values of RQD / J_n.

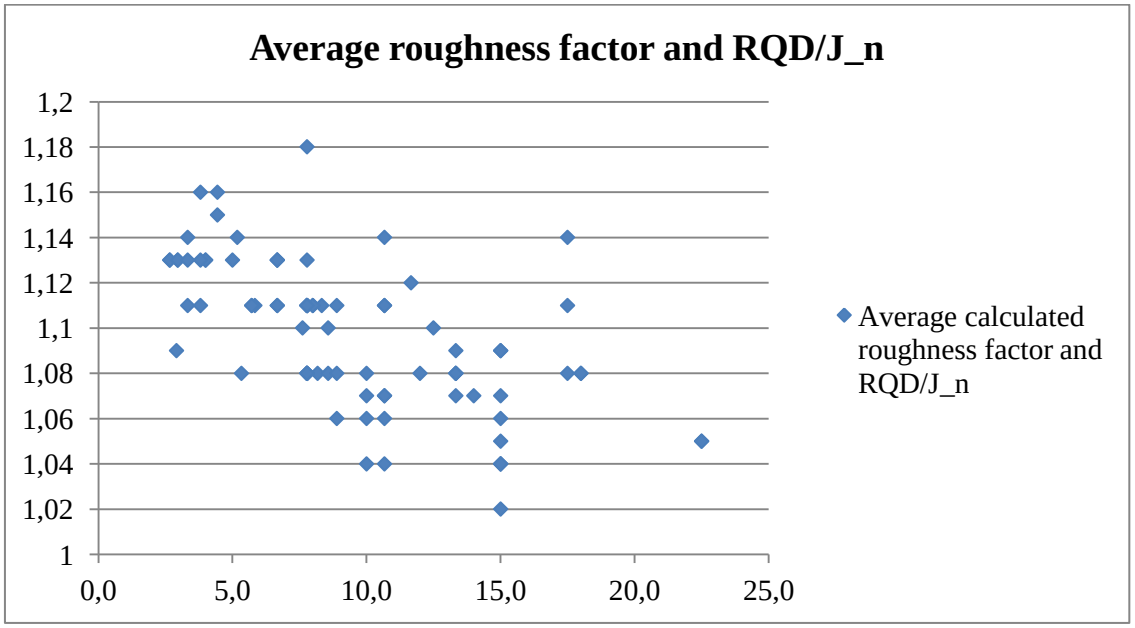

Figure 6- 5: Plot showing the calculated roughness factor and the RQD / J_n quotient. Vertical scale represents the calculated roughness factors and the horizontal scale represents the quotient.

6.3.3 Roughness factor and rock quality designation RQD

The calculated average roughness factor has also been correlated to the RQD parameter in the Q-value. The results are given in Figure 6-5. The vertical scale represents the average calculated roughness factors and the horizontal scale represents the value of RQD.

From the results it is difficult to see a direct correlation between the calculated roughness factor and the RQD, and may be that this plot shows the poorest correlation. The values are more scattered compared to the correlation with the Q-value, and the variations of the values may be too widely spread to be used. But, the result can nevertheless be used as an indication of the

significance of the RQD value. It can to some degree be said that the roughness factor increases with a lower RQD number.

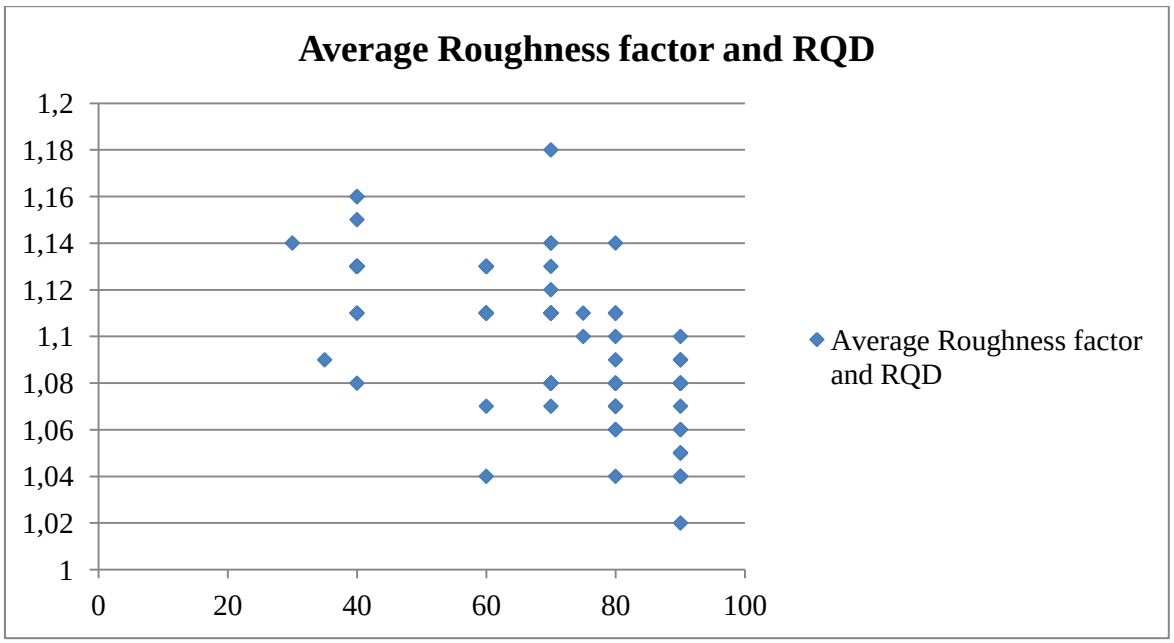

Figure 6-5: Plot showing the correlation between the averages calculated roughness factor and the RQD. Vertical line represents the average roughness factor and horizontal line represents the RQD value.

6.3.4 Roughness factor and the joint set number (J_n)

The calculated average roughness factor has been correlated to the joint set number J_n. This is to see if the number of fractures can have an influence on the roughness of the tunnel surface and if the joint set number can be used for further provision of the roughness factor. The results can be seen in Figure 6-6.

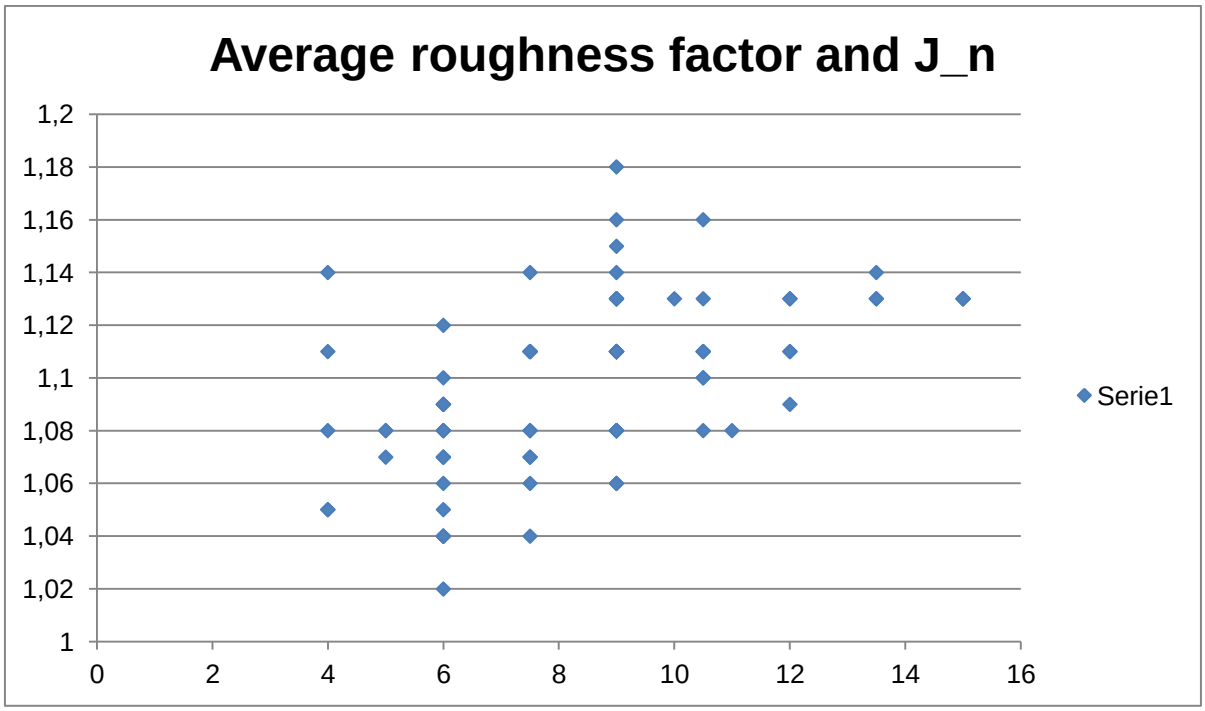

Figure 6-6: Plot of the correlation of the calculated roughness factor and the joint set number J_n. Vertical line represents the average roughness factor and horizontal line represents the value of the joint set number J_n.

The result generally display large scatter of roughness factor for a given joint set number. For one particular value of joint set number J_n the range of the roughness factor can be up to 0,12. But, it can be seen that the lower limits for the given joint set numbers has a district linear increase. For a joint set number of 6, which represent two joint set plus one random, the average calculated roughness factor is 1,02 and above. For a joint set number of 9, which represent three joint sets, the average value of the roughness factor is 1,06 and above. This indicates that for every additional joint in the rock mass, the value of the roughness factor increases with approximately 0,04.

6.3.5 Roughness factor in weakness zones and with the presence of wedges

The calculated roughness factor has been extracted in one weakness zone in the cavern. As seen from the comparison of the hand mapped data and the LiDAR data it can be determined that the nature and structure of the tunnel surface is about the same for both the zones. Therefore it can be assumed that the roughness calculated from the weakness zone 134 to 143 also can apply for the weakness zone at Chainage 199 to 206.

The calculated roughness factor for the weakness zone lies between 1.14 and 1.16. The calculated roughness factors for all extracted profiles are listed in Table II-1 in the Appendix II, and the calculated roughness factors extracted for profiles between 134 to143 and 199 to 206 are provided in Table II-2 and Table II-3, respectively. As seen from the results of the correlation between the calculated roughness factor and the Q-value, this can be expected.

It is done a visual analysis and extracted calculated roughness factors of the weakness zone between the chainage no. 138 to 143. There is also detected and mapped a weakness zone between the chainages no. 199 to 206. Calculated roughness factors for chainages no. 199 to 206 have not been performed but from the comparison in Section 5-1 it can be anticipated that the properties from the weakness zone at chainage no. 138 to 143 also can apply for the zone at chainage no. 199 to 206.

In two different areas it has been detected wedges and the calculated roughness factor has been extracted for both these sections. Two wedges are discovered in the roof at the slash near the chainages n. 169 to 185. Figure 6-7 shows a profile of the wedge by chainage no. 185. The calculated average roughness factor in profiles of the slash near chainage no. 180 and 172 is 1,10. The calculated average roughness factors for these profiles are presented in Table II- 2 in Appendix II.

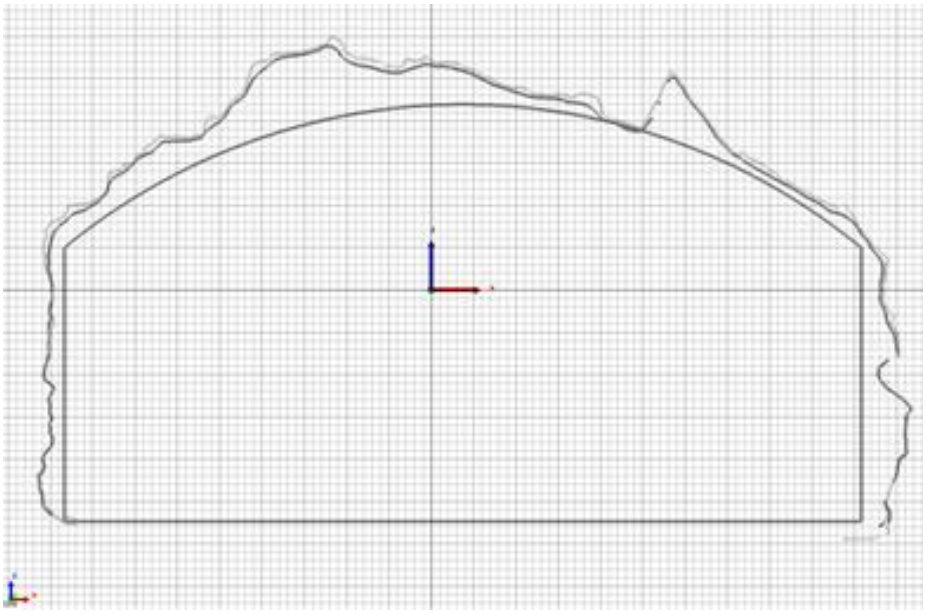

Figure 6-7: Profile of the wedge at chainage no. 185.

6.3.6 Roughness factor within small scale roughness, large scale roughness and both

It has been done an evaluation of the profiles consisting of small scale roughness and large scale roughness and also profiles which have a combination of small scale and large scale roughness. This has been done by selecting profiles which exhibits small scale roughness and calculating an average roughness factor for these profiles. This is also performed for profiles with dominating the large scale roughness and for profiles with a combination of these two. It was only extracted one profile with both large and small scale roughness, so this value is no average calculated from several measurements. The same must be mentioned about analyzing small scale and large scale roughness. It was analyzed 5 profiles with small scale roughness and 4 profiles of large scale roughness. The calculation has been done to evaluate the differences between the small and the large scale roughness.

Table 6-4 presents the results of the calculation of the average roughness factors for the small scale roughness, large scale roughness and the combination. The results indicate that the roughness factor is larger for dominating small scale roughness than large scale roughness. The roughness factor calculated for the combination of the two is higher that the roughness factors of the small scale and the large scale separately.

Table 6-4: The results of the average calculated roughness factor for small scale roughness, large scale roughness and a combination of these two.

Small scale roughness	Large scale roughness	Combination
1,16	**1,1**	**1,18**

As mentioned it was only extracted one profile which included small scale and large scale roughness combined. Due to this the roughness factor presented in the table should not be taken as a representative value.

6.4 Creating and calibrating a look-up-chart for estimating the roughness factor in tunnel applications

This section will present the results from the evaluation described in Section 5-4 of creating and calibrating a lookup-chart for estimating the roughness factor for a better calculation of the sprayed concrete volume. This includes selecting parameters of importance, determining specific values for the roughness factors and also present suggestions of look-up-charts. In addition it is suggested methodologies for further use of the Lidar scanning system for estimating the roughness factor in tunnel applications.

6.4.1 Selecting parameters for calibrating the look-up-chart

For creating and calibrating a look-up-chart for estimating the roughness factor a selection of important parameters has been done. The parameters chosen are based on the results from the analyses in the Sections 6-1 to 6-3.

The results from the correlation between the calculated roughness factor and the Q-value for the corresponding areas from the Section 6.3.1 seem to show the strongest correlation and therefore give the most reasonable starting point for further analysis. It can be anticipated that the Q-value can be an indication of the difference in the roughness of the rock mass surface.

One other important factor for the roughness of the tunnel surface is how well the tunnel is blasted. Careless blasting tends to cause more fractures and joints in the rock mass and hence more roughness in the surface. The significance and the connection between the roughness factor and the blasted surface are not evaluated in this thesis, and are not taken into account in the suggestions of the look-up-chart.

Based on the argument above it is decided to use the Q-value as a basis for the calibration of the look-up-chart. In addition it is chosen to use the number of joint sets. This is based on the assumption that the presence of wedges can have a connection with the number of fractures in the rock mass.

6.4.2 Determining values for the suggested look-up-chart

A selection of values and boundaries of the roughness factor has been performed, based on the correlation performed in Section 6.3.1. As a basis for the look-up-chart the average value of the

calculated roughness factor for the corresponding Q-value is used. This is done by adding a trend line for the points presented in the form Figure 6-7 below, and selecting roughness factors for the corresponding rock mass quality. In addition it can be seen from the correlation of the joint set number and the calculated roughness factor that the roughness factor generally increases every increasing value of the joint set number, as seen in the Figure 6-8. It is based on this determined that these values are used in the calibration of the look-up-chart.

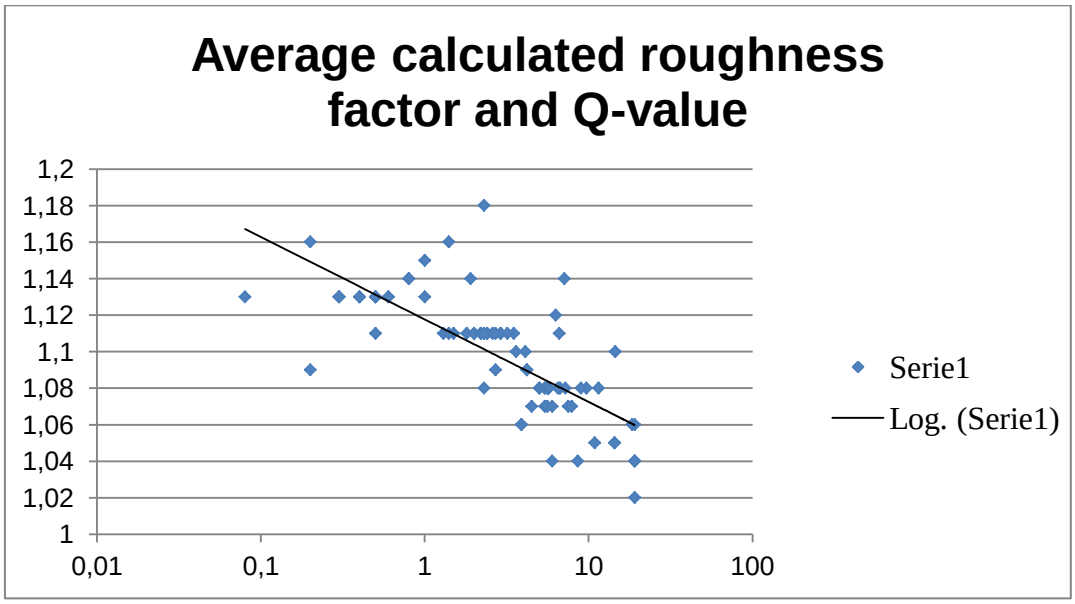

Figure 6-7: Calculated average roughness factor for a given Q-value. The line is representing an estimated trend line. Note that the horizontal scale representing the Q-values is logarithmic.

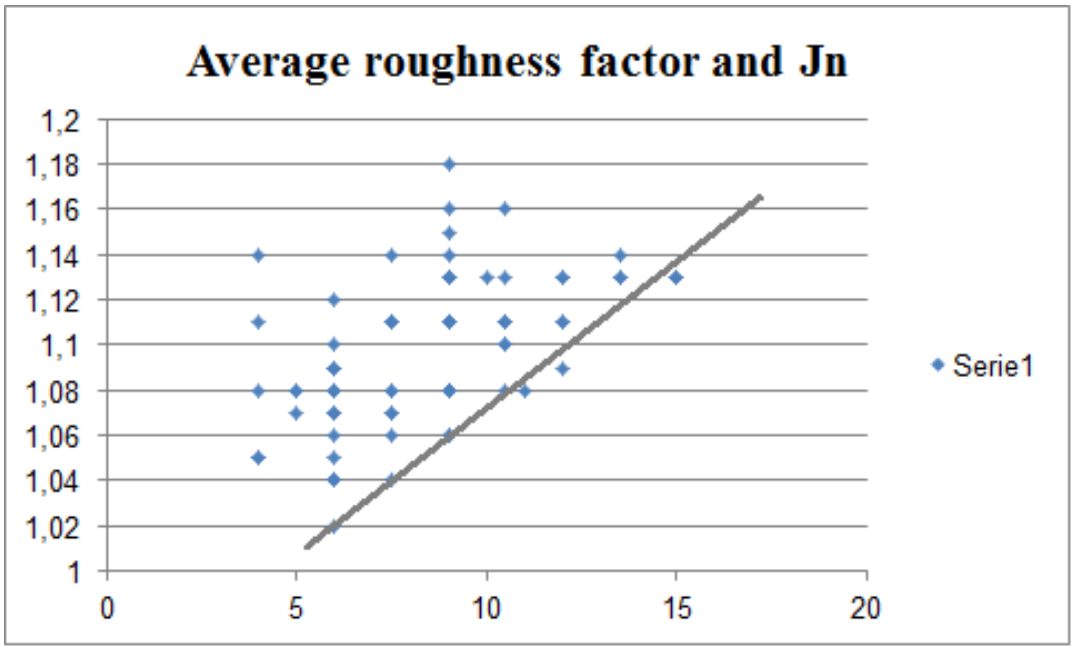

Figure 6-8: Calculated average roughness factor for a given joint set number. The line is representing an estimated trend line.

Based on the charts above, a suggestion of the values of a look-up-chart is presented in Table 6-4. The rock mass quality classes F to B are presented from the left to right horizontally in Table 6-5. The values of the roughness factors corresponding to a given rock mass class is extracted from the trend line presented in Figure 6-7. The joint set number is presented in the vertical section on the right side of the table. The values for a given joint set number are extracted from the line presented in Figure 6-8. The suggested roughness factor given in the grey area of the table is found by multiplying the roughness factor for a given rock mass class to the factor suggested for a given joint set number. For example, for a rock mass quality of class D and a joint set number of 9 it can be suggested to use the roughness factor 1,18 for sprayed concrete volume calculations.

Table 6-5: Suggested look-up-chart, based on the results of the comparison of the surface before and after applied sprayed concrete.

1,56	1,50	1,44	1,42	1,38	1,3	15
1,31	1,25	1,21	1,19	1,16	1,09	12
1,27	1,22	1,18	1,16	1,12	1,06	9
1,22	1,17	1,13	1,11	1,08	1,02	6
1,21	1,16	1,12	1,10	1,07	1,01	4
1,2	1,15	1,11	1,09	1,06	Factor	**JOINT SET NUMBER**
F	**E**	**D**	**C**	**B**		
ROCK MASS QUALITY CLASS						

7 Discussions

This chapter will discuss the results presented in Chapter 6. The discussion will be focusing on answering the objectives in Section 1.4. It will address the issues around using the LiDAR scanning system for mapping and visualizing geological features on the tunnel surface. It will also address the methods used and the results of the calculation of the roughness factor for every blasted round and the correlation between the calculated roughness factors and geological features for the corresponding area. At last, it is discussed the results of the creation of the look-up-chart, together with it limitations and errors.

7.1 Comparing geological features from manually mapped data to the LiDAR data

From the comparison of the hand mapped data and the Lidar data is has to some extent been possible to recognize geological features on the tunnel surface. The Lidar model was able to visualize the wedges and identify the planes that define the shape of the wedges. The model can also distinguish joints and fractures. The wedges detected were of different volumes but had a distinguished direction and shape. This was also described in the hand mapped data. The images from the hand mapped data and the LiDAR data both show the directions and the lengths of these fractures but due to inaccuracy with measuring and drawing by hand the hand mapped data may differ slightly in place and direction from the LiDAR data. The LiDAR data is projecting the true surface of the tunnel and the accuracy of the mapping done by LiDAR is based on the resolution given before the scanning takes place. This was discussed in Section 3.1.

7.1.1 Detecting major structures and geometry

The comparison performed near chainage no. 242 shows that the LiDAR data could not detect the folded and metamorphosed pegmatitic belts. A seen from the picture the belt is highly irregular and strongly folded. Even though the meshed model of the rock surface did not show a distinct different between the belts of pegmatite in magmatic rock mass it is known that detecting structures in LiDAR data is possible (Haugland 2010). One reason for not detecting the belts can be that the model used for this analysis was displayed as a meshed model. If the LiDAR model

were visualized in a point cloud with intensity values, it may have been easier to detect structures. The meshed Lidar model is not able to detect differences between the belts and the surrounding rock mass because there is no intensity value in the meshed model.

The wedges on the other hand were easier to detect with the meshed model. The pictures presented in Figure 6-2 and 6-3 shows a good agreement between the model of the surface with LiDAR and the mapping conducted by the engineering geologist on site. The small variation of the location of the wedges drawn in the hand mapped data compared to the LiDAR data is because of the hand mapped data is more inaccurate due to human inaccuracies.

7.1.2 Detecting weakness zones

From the comparison of data of the weakness zone it was mentioned that is was difficult to distinguish the weakness zone from the surrounding rock mass. The rock mass in the weakness zones are highly brecciated and crushed and the roughness of the surface is high. The weakness zones appear in sections with already very poor rock mass quality. Surfaces with very poor rock mass quality displays a very rough nature and therefore it can be difficult to distinguish the weakness zones from the surrounding rock mass.

Weakness zones usually differ from the surrounding rock mass structure by being very or extremely crushed. In some cases it can be a distinguished a separation between the weakness zone and in other cases a gradual transition. The weakness zones in this cavern were in sections with poor rock mass quality which was already crushed and brecciated. This may be a reason why it was difficult to separate the weakness zones from the surrounding rock mass. In addition the rock mass being of metamorphic rock and with no distinguished foliation pattern could have made it more difficult to detect the zones.

The 3D model used in this thesis was a meshed model. If the model was visualized as a point cloud it is likely that the weakness zones could be detected.

7.1.3 Errors associated with the LiDAR model

Parameters like intensity and resolution may, as mentioned previously, be of importance. The resolution is determined before the scanning of the surface and determines the range of what the scanner can “see”. If the resolution is small the meshed model gives a more representative and correct image of the tunnel surface, and leaves the range of error at a minimum. But on the other

hand it returns a lot of data and makes the data unmanageable. The intensity value is determined before the scanning of the surface.
It can be beneficial to adjust the resolution compared to the range of error set in the processing stage. These can maybe reduce the number of small holes in the profiles. Holes are also due to occlusion. Especially when scanning a surface only once.

7.2 Calculated roughness factors from applied sprayed concrete

It has been performed a calculation of the roughness factor for every blasted round between the chainages no.126 and 194 and chainages no. 291 and 325. The calculation is done to evaluate the rough nature of the tunnel surface and to see if it can be a connection of the calculated roughness factor and the rock mass quality of the corresponding sections. The method used for extraction of profiles will be evaluated and discussed together with the values for the calculated roughness

7.2.1 Calculated roughness factor using the profile length

The results of this analysis are presented in Section 6.2.1. The assumption is that the profile length measuring is the best method for calculating the roughness factor. During the process of measuring the profile length it has been discovered that this method takes a very long time. This was due to the many holes in the model. The 3D model consists of many holes, both large and small and makes the model not watertight and thus the profiles not continuous. The measuring of the not continuous lines were performed in a very cumbersome way and usually it could take up to 2 hours to measure and extract one average roughness factor for one blasted round. The measuring of these profiles were carried out by measuring the continuous lines and creating an "as if" line in the holes in between. This does not give the true length of the cross section but it keeps the errors to a minimum.

Areas with too many large holes were attempted left out from the analysis. Creating lines between the continuous lines did not take up too much time, but the lines do not represent true rock mass surface and the uncertainties increases. It was the many small holes which made the process time consuming. Small holes are in this context considered to be around 10 – 20 cm. Creating "as if" lines in the small gap between the lines generated in the cross section were a challenging process. The small gaps keep the error at a minimum, but the time used for the filling increases.

Due to the holes in the profiles, it must be taken into consideration the range of error in the measured length, and hence the calculated roughness factor. It cannot easily be drawn a line between the gaps, because this line will not represent the true surface of the rock mass. If in example the "as if" lines were drawn in a highly brecciated area it would be as a straight line and not as a line representing the true surface. The length of the cross section may be measured wrong and this may lead to wrongly calculated roughness factor for the profile and hence wrong value for the average roughness factor for the blasted round.

Calculated roughness factors

As seen from the results in Table 6-1 in Section 6.2 and in Table II-1 to II-3 in Appendix II the calculated roughness factors are highly variable. First of all the values of the calculated roughness factor from the slash is higher than the pilot. This can be the caused by the difference in geology for the two sides of the cavern. Second, the calculated roughness factors within the same area i.e. the chainages between no. 130 and 159, as the geology appears to be uniform from 1,08 to 1,18. This is in this context considerable due to the apparently uniform geology. Upon closer investigation it must be said that the 3D model of the blasted round near chainage (no. 148) with a roughness factor of 1,08 could show the boreholes of the blasting on the surface and this may be the reason for a relatively small roughness factor. The chainage (no. 159) with the value 1,18 is consisting of a large wedge. These characteristics could be seen in the slash for the same chainages, but to a lesser extent at the other sections. So it can based on this be mentioned that the highest variation in the calculated roughness factor can be found in sections which consists of poor rock mass quality.

The number of calculated profiles for each blasted round is also highly variable. From the Chainages 169, 174, 296 and 311 it has only been measured and calculated two roughness factors. Many profiles were extracted from the whole blasted round but the polylines representing the rock surface were not continuous. This was due to a large number of holes in the 3D model. Typical for these blasted rounds was that there were several rock falls from the roof and cases of double and triple polylines. This is discussed in section 5.2.3. Because it is only used two calculated roughness factors to extract the average it must be mentioned that the average value may not be the most representative one. But at the same time the values used to extract the average value does not have a great range. It can also be mentioned that the calculated average

roughness factor in this thesis may be smaller than the roughness factors used in tunnel applications.

From the table in the Appendix II it can be seen that some of the measured lengths are shorter compared to others. In some areas the sprayed concrete model did begin 4 to 6 meters above the tunnel floor. These lengths are still included in the comparison because the roughness factor for the profile still can be representative if the measuring of the rock mass length begins at the same height of the wall.

It can also be registered that the roughness factor is generally larger for "the slash "than the pilot. This may be caused by unfavorable crack orientation and rock falls which are more prominent in "the slash "than in the pilot.

7.2.2 Evaluation of the method used for calculating the roughness factor

From the results of the calculated roughness factors in Appendix II, some of the calculated roughness factors are very small. In some cases the value is as low as 1,01. This must be taken in to consideration when using the average value further in this thesis. This low value may be due to imprecise measurements of the profile lengths. Imprecise measurements may be caused by a large amount of small holes in the model which again leads to a large degree of error in the results. In addition it could in some areas be seen a high degree of small scale roughness on the sprayed concrete model. It is believed that increasing degree of small scale roughness causes a larger area of the surface and hence a larger profile length, which again leads to a larger roughness factor. If a rock mass has very rough nature it would assumingly give a high roughness factor. If the roughness of the sprayed concrete is high it may lead to a smaller roughness factor, and may not be the "correct" roughness factor for the actual area. The nature of the surface of the sprayed concrete should assumingly be quite smooth. The large roughness of the sprayed concrete may be caused by multiple lines from two or three scans, which have been aligned, edited or meshed properly.

As mentioned earlier, the meshed model has some holes. The pilot and "the slash "were scanned separately, producing separate point clouds. This can cause the difficulties with aligning the point cloud from "the slash "to the point cloud of the pilot and previous blasted rounds. The holes are particularly visible in the transition between the slash and the pilot in the LiDAR data, and can in

some cases be quite large. These holes do not give a good representation of the actual tunnel surface and can give an incorrect surface area and thus an incorrect roughness factor.

Small scale and large scale roughness

From the calculated roughness factors it can be seen that the surface with the larges roughness is for poor rock mass quality. What most characterizes the poor rock mass qualities is the amount of small scale roughness. It must be mentioned that applying sprayed concrete to a surface with small scale roughness requires a larger amount of sprayed concrete. The holes will fill up first and then the surface as a whole unit. Surfaces with a large roughness may require a less amount of sprayed concrete to cover the surface. So based on this it must be questioned whether the calculated roughness factor is the "correct" roughness factor recommended in tunnel applications. It may look like the small scale roughness generates a much higher roughness than the large scale roughness. This is tried to explain in the figure 7-1 below. The figure illustrates on top small scale roughness and at the bottom large scale roughness. The calculated roughness for the large scale roughness is much lower and the amount of sprayed concrete needed to fill the cavities is lower due to that the sprayed concrete does not fill up the large caves but be covered with a thin layer. This may support whether the method used for estimating the roughness factor in this thesis is the correct method used.

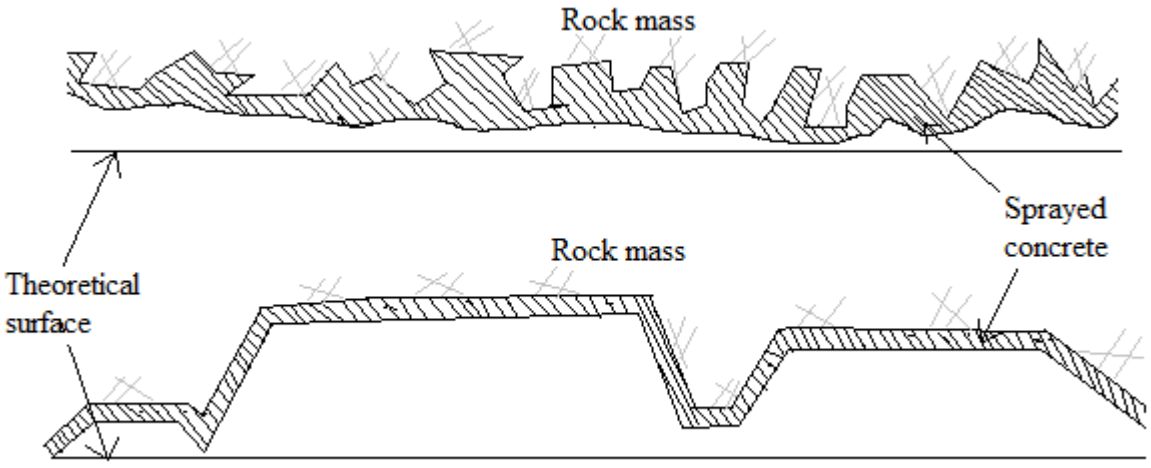

Figure 7-1: Small scale roughness on top and large scale roughness below.

7.3 Develop methodologies using Lidar data for estimating the roughness factor

The method used in this thesis will be assessed to find its suitability for developing methodologies for estimating the roughness factor. It has been performed correlations between the calculated roughness factors and different geological features, especially with respect to parameters in the Q-system. This was done to investigate which parameter is most suitable for further work in creating a look-up-chart.

7.3.1 Correlation between the roughness factor and the selected parameters

The assumption is that the average calculated roughness factor may have a connection with the Q-value. From the results of the comparison it can be assumed that the roughness of the surface may be correlated to the rock mass quality. Generally it can be said that the calculated roughness factor increases with decreasing rock mass quality.

The overall structure of the rock mass can have an impact on the stability of the rock mass. From Section 2.2 the importance of the fractures pattern in the rock mass was emphasized. The Q-value itself do not provide a description of the roughness of the surface, but the RQD / J_n quotient, is a measurable value and was therefore an interesting parameter to evaluate. As seen from the result it can be said that the calculated roughness factor did not correlate well with the quotient. The values are more scattered and do not provide give a clear correlation to the roughness factor. It can still be seen an indication that the roughness factor increases with a decreasing value of the RQD / J_n. In the correlation with the roughness factor and the RQD it was also seen that the values were scattered and did not give a clear indication of a distinct value of the roughness factor for a given RQD. This may be a surprise since it can be anticipated that a rock mass which consists of a high degree of jointing may display a higher surface roughness. The correlation with the most distinct trend is between the roughness factor and the joint set number. From the result in Figure 6-6 it can be seen that the variations of the roughness factors for a given joint set number are quite large. In spite of the variation it can be suggested that the lower value of the roughness factor follows a certain gradient and it seems that the value of the roughness factor increases with the value of about 0,2 to 0,3 for every joint set number. Based on this the joint set number were taken in to further analysis.

The results of the calculated roughness factor from the weakness zone are as anticipated. The overall quality of the rock mass in the zones is generally low and the results from the calculations show that the roughness factors are higher for lower rock mass quality. The analysis of the weakness zones performed in Section 6.3 showed that the Lidar did not display a distinct difference between the weakness zones and the surrounding rock mass. The calculated values of the roughness factors also display this. Also the roughness factors for the areas containing wedges are quite high. The wedges were in area with fair rock mass quality and this must be taken more into consideration in further work.

Limitations of the correlations

This analysis is performed in one single cavern. The purpose of the correlation is to find parameters of significance for creating a look-up-chart. The amount of data used in this correlation is very limited. First of all the cavern consists of one type of rock mass, so the limitations are that the correlations only apply in metamorphic rock. For example in sedimentary rock mass it can be distinct bedding and this was not seen in this cavern. Secondly, the number of profiles analyzed is also limited. The cavern is quite large and due to the amount of time spent on measuring these profiles, the analysis was divided in sections based on similar geology. This made the amount of data even smaller. At last, the number of weakness zones and wedges investigated are too small to give an indication of the connections between the roughness factors. This suggests further investigations for other types of rock masses, rock mass qualities and features and in addition weakness zones and wedges.

Evaluation of the method used

Using a LiDAR model of the surfaces before and after applied sprayed concrete for estimating the roughness factor has been proven useful. The model in PolyWorks represents the true surface of the rock mass and the measured profile lengths represent the actual lengths in the generated profile. This is useful because the calculated roughness factor represents the true roughness factor for the actual surface. Therefore it was suggested to develop methods for using the Lidar data for determination of the roughness factor.

Working with the model in PolyWorks a few challenges arose. Since the Lidar model of the rock surface was not completely watertight, the lines representing the rock surface from the generated profiles consisted of several small and at times large holes. This made first of all the lines not representable for the actual surface and secondly measuring these lines and adding them together was very time consuming. It was also made an attempt to export the profile lines into ArcGIS Software but the same problem was encountered. The lines consisted of many discontinuous lines whish had to be added together.

After working with this method it must be discussed whether the method used for extracting the roughness factor may be effective or not when it comes to tunnel applications. It may be recommended to investigate alternative methods for this purpose. Since the roughness factor needs to be established after each blasted round, the roughness factor calculated with the Lidar data also needs to be estimated for every blasted round. This can be done by finding the area roughness for the actual surface. Haugland (2012) suggested an area roughness factor by dividing the area of the surface by the area of the theoretical surface area. Instead of extracting cross sections and measure profile lengths it can be interesting to calculate the area roughness by dividing area of the rock mass surface by the area of the sprayed concrete surface.

After measuring and calculating the roughness factors it was made a suggestion to use the correlation between the calculated roughness factor and the Q-value together with the joint set number for further use. This suggestion was made due to the wish of at some point incorporate the calculated roughness factors in to the Q-system. Based on the amount of data used in the correlation it can at this point be difficult to determine if this is a correct method. Both since the correlations were not unambiguous but also because the data sets used in the correlation are too small. Therefore it can be beneficial to use bigger data sets and explore several different types of geology before deciding whether the method used is correct or not. In addition, it can be interesting to explore if it can exist other relationships with the roughness factor. This may include the effect of crack orientation has on the profile and also the blasting quality on the rock mass surface.

7.4 Creating and calibrating a look-up-chart for estimating the roughness factor in tunnel applications

A suggestion of a lock-up-chart is made based on the results of the correlations performed in Section 6-3. An assessment of the results of the lock-up-chart has to be evaluated.

7.4.1 Creation of the look-up-chart

The suggested lock-up-chart presented in Table 6-4 is made only on the basis of the results of this thesis. It is anticipated that the Q-value is essential for the roughness factor for rock mass surfaces. It is further anticipated that the joint set number can have an impact on the roughness factor. This may have some limitations. It is mentioned in the previous section that there can be other important parameters which also needs to be taken in to consideration when creating the lock-up-chart. Especially one parameter that may be further investigated is the blasting quality. This can be highly variable and does not need to have a connection to the rock mass quality. A poor rock mass quality poorly blasted has a different roughness on the surface than a good blasted surface. This variation needs to be taken in to consideration when creating the lock-up-chart.

The analyses of the cavern consisted of extracting roughness factor for different types of rock mass qualities. The rock mass qualities in the analyses range from B to F. This leaves the rock mass qualities A and G not investigated. Therefore, a suggestion of roughness factor for these rock mass qualities cannot be established. Based on this it must be pointed out that this chart is incomplete and it is recommended not to use it as it is now. The Q-system as mentioned in Section 2.1 includes about 2000 test sites, and has been developed over several decades. If the presented look-up-chart is at some point suggested incorporated in to the Q-system, it must be performed many more analyses on several test cases. This also includes a calibration of the values of the roughness factors, the boundaries and which parameters to be used. But it can be used as a basis for further investigations.

8 Conclusions and future work

The thesis provides an assessment and suggests factors that may affect the surface roughness of a rock mass. This includes an evaluation of the correlation between the calculated roughness factor and the Q-value for the corresponding blasted round. Furthermore it has been discussed other characteristics that may affect the roughness factor. Based on this a look-up-chart has been suggested to provide an easier determination of the roughness factor for sprayed concrete volume calculations. It has also been made suggestions on the values and the boundaries for an easier determination of the roughness factor. Measurement errors and limitations of the study have also been addressed.

8.4 Conclusions

The look-up-chart providing an easier determination of the roughness factor for sprayed concrete volume calculations have been difficult to establish. This is mainly because of the limitations of the study due to one single test case, and will not provide general representative values for other types of geologies. The Q-system is calibrated from several different test cases and it is therefore not correct to incorporate the calculated and recommended roughness factors in to this system. More investigations need to be made.

The average roughness factors calculated for each blasted round show some correlations to the Q-value for the corresponding section. It can generally be said that the calculated roughness factor increases with decreasing rock mass quality. This can be shown both from the correlation plot and the calculation of the average roughness factor for each rock mass quality class. At the same time wedges and blasting quality also seem to have an impact on the roughness factor. The wedges have been discussed in this thesis, but the amount of data is insufficient to make suggestions of in what way it correlates with the roughness factor.

The results of the comparison of the LiDAR data and the manually mapped data, suggests that the meshed 3D model is not capable of recognizing and visualizing geological structures, but it can detect geometry in terms of wedges and rock falls. It can detect to a certain extent weakness zones in terms of its heavily crushed and brecciated nature of the surface. In addition fractures and its orientation can be detected.

The proposed method for calculating the roughness factor is a possible method of extracting the roughness factor. Making cross sections in the 3D model in PolyWorks is a valuable application for extracting true profile lengths of the rock mass surface. The method used in this thesis may yet not be efficient. The calculated roughness factor is based on the profile length of the rock mass surface divided by the sprayed concrete profile length. Since the roughness factor needs to be established for every blasted round it can be convenient to calculate the area roughness by dividing the area of the rock mass by the area of the sprayed concrete.

8.5 Further work

The most important limitation of the study is the number of test cases used in this thesis. The results imply that there is a possible a correlation between the roughness factor and the Q-system. To verify this it requires additional analyses on several different types of rock, such as sedimentary and volcanic rocks. In addition, this study was performed in rocks with very poor, poor and fair rock mass quality. This excludes analyses of extremely to exceptionally poor, and also of very to exceptionally good rock mass quality. For further work it is recommended to perform analyses on several different test cases with different types of geology, rock mass quality and joint directions, and develop a look-up-chart for a broader set of data.

The method used for calculating the roughness factor for each blasted round was the most time consuming process in this task. It could be a solution to calculate the roughness factor by using area roughness instead, but that requires that the model is completely watertight. This again is controlled by the processing of the LiDAR data and the time it takes from scanning a surface to visualizing and analyzing the same surface in PolyWorks takes much time. The time needed for processing the data will decrease with further software developments making more user-friendly applications.

The presences of wedges also seem to be important for determining the roughness factor. It is the cavities that will fill up first, and the peaks will be covered last. To fulfill the requirements of minimum sprayed concrete thickness means that the volume needed is large. Since the application of the sprayed concrete should be performed perpendicular to the surface it can be of interest to make an assessment on the significance of the angle between the surfaces in the wedges.

The rock mass surface highly depends on the drill and blast process in the tunnel. Further studies should therefore also be conducted to evaluate the influence of poor blasting in tunnels and how this again can affect the roughness factor.

References

Arayici, J., 2007. *An approach for real world data modeling with the 3D terrestrial laser scanner for built environment.* School of Construction and Property Management, University of Salford, United Kingdom, Article pp 24.

Barton, N., Lien, R. and Lunde, J. 1974, *Engineering classification of rock masses for the design of tunnel support*. Rock Mechanics 6.

Brock E. and Nilsen B. 2001, *Ingeniørgeologi – Berg*, Compendium in rock engineering, Institute of geology and rock mechanics, Norwegian University of Science and Technology.

Carstens, H. 2007, *The Reason why Hanekleiv Tunnel Collapsed*, Article in GEO Magazine pp. 40-41, [Accessed 25.09.2013] Available at http://www.geo365.no/sfiles/4/47/4/file/hanekleiv40.pdf

FARO 2013, Laser Scanner Faro Fokus 3D. *Applications for Architecture and Civil Engineering.* [Accessed 20.09.2013]. Available at http://www.faro.com/products/3d-surveying/laserscanner-faro-focus-3d/applications

Fekete, S., Diederichs, M., Lato, M., 2010, *Geotechnical and Operational Applications for 3-dimensional Scanning in Drill and Blast Tunnels.* Tunneling and Underground Space Technology. Article pp. 614-628.

Gigli, G. and Casagli, N., 2010, *Semi-Automatic extraction for rock mass structural data from high resolution LIDAR point clouds.* International Journal of Rock Mechanics and Mining Sciences, pp. 188-198.

GIM International 2009, Laser Scanning in Deformation Measurements, Volume 23, Issue, [Accessed 01.12.2013], Available at http://www.gim-international.com/issues/articles/id1292-Laser_Scanning_in_Deformation_Measurements.html

Grimstad, E. and Barton, N., 1993, *Updating of the Q-System for NMT*. Proceedings of the International Symposium on Sprayed Concrete. Modern Use of Wet Mixed Sprayed Concrete for Underground Support, Fagernes, Norway.

Hadjigeorgiou, J. and Charette, F., 2001, *Rock Bolting for Underground Excavations*, Society for Mining, Metallurgy and Exploration, Chapter 63.

Harrap, R. and Lato, M. 2010, *An overview of LiDAR; collection to applications*, Article, [Accessed 01.12.2013], Available at http://www.ngi.no/upload/48594/1%20What%20Is%20Lidar.pdf

Haugland, H.H., 2010, *Terrestrial LiDAR in tunnels under construction*. A study of potential use for engineering geological- and operational applications, and work-flow design for data acquisition and processing. Master thesis in Geosciences. University of Oslo.

Hoek, E., Kaiser,P.K., Bawden,W.F., 1993, *Support of underground excavations in hard rock*. pp 20-26.

InnovMetric. 2013. PolyWorks v13, [Accessed: 10.11.2013]. Available at http://www.innovmetric.com/polyworks/3D-scanners/home.aspx?lang=en

Kemeny, J. and K. Turner. 2008, *Ground-Based LiDAR: Rock Slope Mapping and Assessment*, Report FHWA-CFL/TD-08-006, Federal Highway Administration Central Federal Lands Highway Division, Lakewood, CO.

Lato, M. and Diederichs, M. 2010, *Bias Correction for View-Limited for LiDAR Scanning of Rock Outcrops for Structural Characterization*, Rock Mech. Rock Eng. pp. 616 – 619.

LiDAR UK, 2014. The applications of LiDAR scanning system, [Accessed at 22.01.2014] Available at: http://www.lidar-uk.com/usage-of-lidar/

Løset, F. 1997. *Practical use of the Q – method*. Norwegian Geotechnical Institute, 592026-4. 41 pp

Mechelke, K., Kersten, T.P., Lindstaedt, M., 2007, *Comparative investigations into the terrestrial behavior of the new generation of the terrestrial laser scanning systems.* Optical 3D Measurement Techniques, Department Geomatics, HefenCity University Hamburg, pp. 319 – 328.

Morgan, Elin K., 2012. *Nedre Romerike Vannverk, Nytt høydebasseng*, Ingeniørgeologisk sluttrapport, Norwegian Geotechnical Institute, 20101064-00-6-R 14 pp.

Morgan, Elin K. and Lato, M 2010. *LiDAR under constructions: A case study from a water storage cavern, Norway.* Norwegian Geotechnical Institute, Oslo, Norway. 9 pp.

Myrvang, A., 2001, *Bergmekanikk*, Compendium in Rock Mechanics, Institute for Geology and Rock Mechanics, Norwegian University of Science. pp 80.

Nilsen, B. 2010. *Cases of instability caused by weakness zones in Norwegian tunnels*, NTNU, Department of Geology and Mineral Recourses Engineering, Article, 6 pp.

Norwegian Association for Blasting Technique, 2008, *The collapse in Ålesund – Why did it happen?* Article, [Accessed at 30.09.2013] Available at http://www.nff.no/article.php?id=254

Norwegian Concrete Association, 2003. *Sprøytebetong til fjellsikring*, Publication No 7.

Norwegian Geotechnical Institute (NGI) 2013a, *Using the Q-System, Rock mass classification and support design*. Handbook.

Norwegian Geotechnical Institute (NGI) 2013b, *Tunnel stability*, [Accessed: 16.10.2013]. Available at http://www.ngi.no/en/Project-pages/Tunnel-stability/Background/

Norwegian Geotechnical Institute (NGI), 2013c, Nedre Romerike Vannverk, project file available at NGI, Project no. 20101064.

Norwegian Public Roads Administration, 2010, *Vegtunneler*. Håndbok 021. 134 pp.

Palmstrøm; A. and Broch, E., 2006, *Use and Misuse of the Rock Mass Classification Systems with Particularly Reference to the Q-system*. Article published in Tunnels and Underground Space Technology, vol. 21, pp 575-593

Palmstrøm, A. and Naas, R. 1993. Norwegian Subsea Tunneling – Rock Excavation and Support Techniques. *Int Symposium on technology of bored tunnels under deep waterways*, Copenhagen, Denmark.

Pesci, A., Teza, G., Bonali E., 2011, *Terrestrial Laser Scanner Resolution: Numerical Simulations and Experiments on Spatial Sampling Optimization*, Remote Sensing, Article, pp. 167-184.

Pesci, A., Loddo, F., Confort, D., 2007, *The first terrestrial laser scanner application over Vesuvius*, High Resolution Model of Volcano Crater, International Journal of Remote Sensing 28, pp. 203-219.

Sturzenegger, M. and Stead, D. 2009. Close range terrestrial digital photogrammetry and terrestrial laser scanning for discontinuity characterization on rock cuts. *Engineering Geology* 106, 163-182

Vassilis, G. 2012 *Three-Dimensional Laser Scanning for Geometry Documentation and Construction Management of Highway tunnels during Excavation.* School of Rural and Surveying Engineering, National Technical University of Athens, Article.

Appendix I

Tables of the values for the rock mass class (highlighted with different colors), Q-value, RQD, J_n and RQD/J_n quotient for the different Chainage numbers are provided in Table I-1, Table I-2, Table I-3 and Table I-4 below, respectively.

Table I-1: Table over values used in the correlation between the calculated roughness factor and Q-value, RQD, J_n and RQD/J_n for the different Chainages. The values are for section 1 in the cavern.

	CHAINAGE No.	79	82,5	86,5	91	96	102	107	113	117	123
STROSS	Rock mass class						D		D		D
	Q-value						2,6		2,4		2,9
	RQD						75		70		70
	Jn						9		9		9
	RQD/Jn						8,3		7,8		7,8
PILOT	CHAINAGE No.	79	82,5	86,5	91	96	102	107	112	117	122
	Rock mass class	E	D	C	C	B	B	C	C	D	D
	Q-value	0,6	1,4	9	11,5	14,4	14,4	5	6,6	6,6	2,2
	RQD	70	80	90	90	90	90	80	70	70	60
	Jn	9	9	5	5	4	4	6	4	4	9
	RQD/Jn	7,8	8,9	18,0	18,0	22,5	22,5	13,3	17,5	17,5	6,7

Table I-2: Table over values used in the correlation between the calculated roughness factor and Q-value, RQD, J_n and RQD/J_n for the different Chainages. The values are for sections 2 and 3 in the cavern.

128	135	138	143	148	154	159	164	169	174	179	185	189	194
C	E		E	E		D	C	B	D	C	C	D	C
5	0,2		0,2	0,5		1,9	6,3	14,5	2,7	4,5	4,1	3,6	7,1
80	40		35	40		70	70	75	80	80	90	80	80
6	10,5		12	10,5		4	6	6	6	7,5	10,5	10,5	7,5
13,3	3,8		2,9	3,8		17,5	11,7	12,5	13,3	10,7	8,6	7,6	10,7
126	**133**	**138**	**143**	**148**	**154**	**159**	**164**	**169**	**174**	**179**	**184**	**189**	**194**
E	E	E	D	D	E	D	C	C	C	C	D	C	D
1	0,8	1	1,4	2,3	0,8	2,3	5,4	5,4	4,2	4,2	3,9	5,4	3,9
40	30	40	40	40	70	70	90	90	90	90	90	90	80
10	9	9	9	7,5	13,5	9	11	10,5	6	6	9	6	9
4,0	3,3	4,4	4,4	5,3	5,2	7,8	8,2	8,6	15,0	15,0	10,0	15,0	8,9

Table I-3: Table over values used in the correlation between the calculated roughness factor and Q-value, RQD, J_n and RQD/J_n for the different Chainages. The values are for sections 4 to 7 in the cavern.

199	204	206	213	217	222	227	232	237	242	247	253	259	264	269
E	E	D		D	C	C			C	E	E	D	D	E
0,4	0,3	1,5		2,3	5,6	5,6			5,7	0,5	0,6	1,3	2,9	0,5
60	40	60		60	70	70			70	60	60	70	70	60
15	13,5	10,5		9	9	9			9	9	12	9	9	9
4,0	3,0	5,7		6,7	7,8	7,8			7,8	6,7	5,0	7,8	7,8	6,7

199	204	206	213	218	223	228	233	238	243	248	253	258	263	268
D	E	E	D	D	D	D	E	E	E	C	C	C	C	E
2,4	0,3	0,3	1,8	2	2	2,2	0,5	0,4	0,08	5,7	5,7	5,7	6,7	0,5
80	40	40	40	70	70	60	40	40	40	70	70	70	90	60
7,5	15	15	12	12	9	10,5	10,5	13,5	12	9	9	9	7,5	9
10,7	2,7	2,7	3,3	5,8	7,8	5,7	3,8	3,0	3,3	7,8	7,8	7,8	12,0	6,7

Table I-4: Table over values used in the correlation between the calculated roughness factor and Q-value, RQD, J_n and RQD/J_n for the different Chainages. The values are for section 8 in the cavern.

273	279	284	289	291	298	301	310	315	320	325
D	D	B	C		B		B	B	B	B
3,5	2,7	10,9	9,7		19,1		19,1	19,1	19,1	19,1
60	80	90	80		90		90	90	90	90
7,5	7,5	6	6		6		6	6	6	6
8,0	10,7	15,0	13,3		15,0		15,0	15,0	15,0	15,0

273	278	283	288	291	296	301	306	311	321	325
D	D	C	C	C	C	C	C	C	C	B
3,2	2,3	7,2	6,5	5,6	8,6	7,5	6	6	7,9	18,4
60	70	90	80	80	80	70	60	60	80	80
7,5	9	9	9	7,5	7,5	5	6	6	6	7,5
8,0	7,8	10,0	8,9	10,7	10,7	14,0	10,0	10,0	13,3	10,7

Appendix II

Results of the measured profile lengths from Chainages130 to 159, 164 to 194 and 291 to 325 are presented in Table A-1, Table A-2 and Table A-3, respectively.

Table II-1: Results of measured profile length of the rock surface profile and sprayed concrete surface profile length and the calculated average roughness factors for the

STROSS	Ch 133	Ch 135	Ch 143	Ch 148	Ch 153	Ch 158
Rock profile length	14,23 12,97 13,20 13,69	13,13 17,80 20,66 21,07	18,02 21,74 19,78 20,87 18,24	21,34 20,32 18,37 17,43 17,13	17,95 17,01 16,60 13,44 12,95	19,23 18,67 18,92 18,01 17,93 13,32
Shotcrete profile length	13,69 12,22 12,12 12,24	11,31 15,09 17,70 18,65	16,79 19,86 17,97 18,79 17,02	19,52 18,48 16,14 15,56 15,48	16,71 14,88 15,35 11,79 11,63	17,18 16,29 16,12 15,70 15,82 11,74
Roughness factor	1,04 1,06 1,09 1,12	1,16 1,18 1,17 1,13	1,07 1,09 1,10 1,11 1,07	1,09 1,10 1,14 1,12 1,11	1,07 1,14 1,08 1,14 1,11	1,12 1,15 1,17 1,15 1,13 1,13
Average Roughness factor	**1,08**	**1,16**	**1,09**	**1,11**	**1,11**	**1,14**

PILOT	Ch 130	Ch 138	Ch 143	Ch 148	Ch154	Ch 159
Rock profile length	11,90 17,06 10,40 10,47 12,89	12,89 16,51 15,03 16,12 16,85 14,81 17,40	12,89 11,65 14,94 10,43	8,50 11,95 10,04	11,69 11,47 12,01 12,91 11,33	11,51 10,44 9,16 11,90
Shotcrete profile length	10,19 14,67 8,75 9,47 11,80	11,83 13,88 13,44 13,87 14,75 12,57 14,97	11,64 9,83 12,51 8,91	7,54 11,31 9,39	10,35 10,04 10,41 11,37 10,05	9,53 8,51 7,77 10,83
Roughness factor	1,17 1,16 1,19 1,11 1,09	1,09 1,19 1,12 1,16 1,14 1,18 1,16	1,11 1,19 1,19 1,17	1,13 1,06 1,07	1,13 1,14 1,15 1,14 1,13	1,21 1,23 1,18 1,10
Average Roughness factor	**1,14**	**1,15**	**1,16**	**1,08**	**1,14**	**1,18**

Table II-2: Results of measured profile length of the rock surface profile and sprayed concrete surface profile length and the calculated average roughness factors for the Chainages164 to 194.

STROSS	Ch 164	Ch 169	Ch 174	Ch 179	Ch 185	Ch 189	Ch 194
Rock profile length	11,57 10,17 10,67 10,87	18,57 18,71 17,74 19,58 15,19	19,76 14,16 14,59 15	19 16,06 16,65 20,24 15,23	17,12 17,62 18,85 17,97 15,89	18,39 19,37 18,42 19,88	18,75 18,19 20,07 19,01
Shotcrete profile length	10,98 9,34 9,88 9,92	17,41 17,04 16,9 18,19 13,84	17,7 13,55 13,54 13,49	18,08 14,64 15,47 18,63 13,44	15,65 16,93 17,68 17,45 14,69	17,1 18,15 17,04 18,65	17,49 17,06 19,06 18,26
Roughness factor	1,05 1,09 1,08 1,10	1,07 1,10 1,05 1,08 1,10	1,12 1,05 1,08 1,11	1,05 1,10 1,08 1,09 1,13	1,09 1,04 1,07 1,03 1,08	1,08 1,07 1,08 1,07	1,07 1,07 1,05 1,04
Average Roughness factor	**1,08**	**1,08**	**1,09**	**1,09**	**1,06**	**1,07**	**1,06**

PILOT	Ch 164	Ch 169	Ch 174	Ch 179	Ch 184	Ch 189	Ch 194
Rock profile length	14,46 10,84 14,03	12,65 13,41	13,14 13,49	11,36 12,16 13,14	13,31 13,89 15,55 13,52 14,53	13,5 13,36 13,31 13,95 16,28	15,65 15,62 14,98 11,67
Shotcrete profile length	12,92 9,86 12,36	11,68 12,05	11,84 12,61	10,77 11,19 12,42	12,21 13,09 13,78 12 13,11	12,76 12,14 12,39 11,99 14,7	13,5 13,62 13,39 10,54
Roughness factor	1,12 1,10 1,14	1,08 1,11	1,11 1,07	1,05 1,09 1,06	1,09 1,06 1,13 1,13 1,11	1,06 1,10 1,07 1,16 1,11	1,16 1,15 1,12 1,11
Average Roughness factor	**1,12**	**1,10**	**1,09**	**1,07**	**1,10**	**1,10**	**1,13**

Table II-3: Results of measured profile length of the rock surface profile and sprayed concrete surface profile length and the calculated average roughness factors for the

STROSS	Ch 291	Ch 298	Ch 304	Ch 310	Ch 315	Ch 320	Ch 325
Rock profile length		17,55 17,05 19,98 14,92 15,25		20,02 19,33 19,17	17,89 18,48 18,53	17,41 19,18 19,43	18,41 18,57 16,78 16,64
Shotcrete profile length		16,95 15,92 18,30 14,22 14,37		19,14 18,68 19,32	17,28 17,66 17,98	17,02 18,5 18,51	17,85 18,11 16,68 16,08
Roughness factor	Only shotcrete model	1,04 1,07 1,09 1,05 1,06	Only shotcrete model	1,05 1,03 0,99	1,04 1,05 1,03	1,02 1,04 1,05	1,03 1,03 1,01 1,03
Average Roughness factor		**1,06**		**1,04**	**1,04**	**1,04**	**1,02**

PILOT	Ch 291	Ch 296	Ch 301	Ch 306	Ch 311	Ch 321	Ch 325
Rock profile length	11,5 14,2 12,95	11,35 8,96	12,5 14,77 14,88 14,33	13,16 14,62 14,87 14,35	12,21 14,25	12,43 14,55 15,13 9,12	7,72 9,09 8,38
Shotcrete profile length	10,99 13,39 11,76	11,04 8,54	11,66 13,78 14,09 13,35	12,31 13,61 13,95 13,32	11,63 13,72	11,53 13,39 14,02 8,91	7 8,94 8,01
Roughness factor	1,05 1,06 1,10	1,03 1,05	1,07 1,07 1,06 1,07	1,07 1,07 1,07 1,08	1,05 1,04	1,08 1,09 1,08 1,02	1,10 1,02 1,05
Average Roughness factor	**1,07**	**1,04**	**1,07**	**1,07**	**1,04**	**1,07**	**1,06**